INVESTIGATION OF COMPETITIVE ANTAGONIST BINDING TO THE NICOTINIC ACETYLCHOLINE RECEPTOR USING VOLTAGE-JUMP AND LIGHT-FLASH TECHNIQUES

Thesis by

Mauri Eugene Krouse

In Partial Fulfillment of the Requirements

For the Degree of

Doctor of Philosophy

California Institute of Technology

Pasadena, California 91125

1984

(Submitted May 5, 1984)

ACKNOWLEDGMENTS

I would like to thank my parents, Benjamin and Alyce Krouse, for nurturing my scientific curiosity and I dedicate this thesis to them. I would like to thank Jim Hudspeth for helping me to change fields from physics to biology, and I would like to thank Henry Lester, who taught me electrophysiology, for his constant pressure that led me to discover the methods of scientific research.

I would like to thank my wife, Karen, and my friends, Jeanne Nerbonne and Jeff Segall, for support when I was down and for scientific discussion when I was around. I wish to extend my thanks to Roger Spencer for his assistance with the dissections. Also, I wish to thank those that have supported me over the years: National Research Service Award from NIH, NIH NS 11756, and the Weigle Memorial Fund.

SUMMARY

1. The effect of 2,2'-*bis*-[α-(trimethylammonium)methyl]azobenzene (2BQ), a photoisomerizable competitive antagonist, was studied at the nicotinic acetycholine receptor of *Electrophorus* electroplaques using voltage-jump and light-flash techniques.

2. 2BQ, at concentrations below 3 μM, reduced the amplitude of voltage-jump relaxations but had little effect on the voltage-jump relaxation time constants under all experimental conditions. At higher concentrations and voltages more negative than -150 mV, 2BQ caused significant open channel blockade.

3. Dose-ratio studies showed that the *cis* and *trans* isomers of 2BQ have equilibrium binding constants (K_i) of .33 and 1.0 μM, respectively. The binding constants determined for both isomers are independent of temperature, voltage, agonist concentration, and the nature of the agonist.

4. In a solution of predominantly *cis*-2BQ, visible-light flashes led to a net *cis*→*trans* isomerization and caused an increase in the agonist-induced current. This increase had at least two exponential components; the larger amplitude component had the same time constant as a subsequent voltage-jump relaxation; the smaller amplitude component was investigated using ultraviolet light flashes.

5. In a solution of predominantly *trans*-2BQ, UV-light flashes led to a net *trans*→*cis* isomerization and caused a net decrease in the agonist-induced current. This effect had at least two exponential components. The smaller and faster component was an increase in agonist-induced current and had a similar time constant to the voltage-jump relaxation. The larger component was a slow decrease in the agonist-induced current with rate constant approximately an order of magnitude less than that of the voltage-jump relaxation. This slow component provided a measure of the rate constant for dissociation of *cis*-2BQ

($k_- = 60/s$ at 20°C). Simple modelling of the slope of the dose-rate curves yields an association rate constant of 1.6×10^8/M/s. This agrees with the association rate constant of 1.8×10^8/M/s estimated from the binding constant (K_i). The Q_{10} of the dissociation rate constant of *cis*-2BQ was 3.3 between 6° and 20°C. The rate constants for association and dissociation of *cis*-2BQ at receptors are independent of voltage, agonist concentration, and the nature of the agonist.

6. We have measured the molecular rate constants of a competitive antagonist which has roughly the same K_i as d-tubocurarine but interacts more slowly with the receptor. This leads to the conclusion that curare itself has an association rate constant of 4×10^9/M/s or roughly as fast as possible for an encounter-limited reaction.

TABLE OF CONTENTS

INTRODUCTION

The acetylcholine receptor-complex (receptor + associated ion channel) has been widely studied using physiological (Adams, 1975; Sheridan & Lester, 1977), biochemical (Heidmann & Changeux, 1978; Raftery, 1973) techniques. The polypeptide structure (Raftery *et al.*, 1980) for the acetylcholine receptor has been published and the cDNA for these polypeptides has been cloned (Noda *et al.*, 1983). These studies were conducted using the vertebrate neuromuscular junction, ***Electrophorus*** electroplaques, and ***Torpedo*** electroplaques. As a result of this focus, this integral membrane protein is perhaps the best understood ligand-activated receptor complex.

Pharmacological studies reveal that many compounds bind to the acetylcholine receptor-complex. Some compounds (agonists) bind to a receptor site which induces the complex to open a pore in the membrane. The opening of membrane channels by acetylcholine and other agonists has been extensively studied (Takeuchi & Takeuchi, 1960; Magleby & Stevens, 1972a, 1972b; Anderson & Stevens, 1973; Adams, 1975; Sheridan & Lester, 1977). The kinetics of channel gating have been measured using a voltage clamp and relaxation, noise, or single channel techniques (Neher & Sakmann, 1976). These measurements are possible because when the channel opens, ions flow down their electrochemical gradient producing an electrical signal which can be amplified and recorded. Because the voltage across the cell membrane can be held constant with the voltage clamp circuit, the current measured is directly proportional (a) to the number of channels that open at a given voltage and agonist concentration and (b) to the conductance of the single ion channel. Through techniques such as these it has been possible to study the channel's selectivity for ions, the voltage sensitivity of the channel closing rate constant, and the requirement that two agonists bind

before the channel opens.

The equilibrium agonist-induced current measured in *Electrophorus* electroplaques is dependent upon the opening and closing kinetics for individual receptor-channels (Sheridan & Lester, 1977). One can define a first-order, unidirectional opening rate constant (β') for the agonist-receptor interaction that is dependent upon the agonist concentration and independent of the trans-membrane voltage. Increasing the agonist concentration increases the opening rate constant, and more receptor channels open. Similarly, a closing rate constant (α) can be defined that is voltage dependent, decreasing with hyperpolarization. A decrease in the probability of channel closing that occurs at hyperpolarized voltages leads to an increase in the number of open channels. Therefore, in the presence of agonists a change in either (a) the trans-membrane voltage or (b) the agonist concentration produces a relaxation to a new level of agonist-induced current. This relaxation can be measured and analyzed to give information about the pseudo first-order opening and closing rate constants.

Other compounds (antagonists) bind to the receptor complex and inhibit the opening of the ion channel. Antagonists can be of three different types: (1) competitive antagonists that bind to the closed form of the receptor-channel complex and inhibit agonist binding; (2) uncompetitive antagonists (borrowing terminology from enzyme kinetics) that bind only to the open form of the receptor-channel complex and inhibit the flow of ions through the open channel (local anesthetics are good examples of this kind of antagonist); (3) noncompetitive antagonists that bind to and modify both the open and closed forms of the receptor-channel complex. The binding of the noncompetitive antagonist would interact with the receptor-channel protein and either (a) change the molecular rate constants for agonist binding or (b) reduce the open channel conductance (general anesthetics may fit in this category). At the

vertebrate neuromuscular junction, competitive antagonists bind at or near the acetylcholine binding site (Jenkinson, 1960; Rang, 1971) and, prevent acetylcholine binding and channel opening. The binding of a competitive antagonist to the nicotinic acetylcholine receptor does not induce the channel to open (however, see Morris *et al.*, 1982; Trautmann, 1982 and Morris *et al.*, 1983). Instead, the receptor-channel complex is prevented from binding agonist molecules and opening. As long as at least one competitive antagonist molecule is bound per receptor (Jenkinson, 1960), agonist molecules cannot bind to the receptor-channel complex in the required numbers, and channels do not open. The study of competitive antagonist binding kinetics is of limited use using conventional voltage-clamp techniques because (a) the antagonist-receptor interaction does not directly involve the open state of the channel and (b) the binding constant is not voltage-sensitive. Therefore, voltage-jump relaxations couple only weakly to the antagonist-receptor interaction. Single-channel studies would also yield ambiguous information about the competitive antagonist-receptor interaction. Open-duration histograms would not reveal any components due to the competitive antagonist because competitive antagonists do not open channels nor alter the open channel properties. Closed-duration histograms could reveal the presence of additional components due to the inhibited state of the receptor. In the simple agonist-receptor interaction the assignment of a definite component to the unoccupied-receptor state has not been reported. Therefore, the addition of 1-3 small amplitude components, due to the inhibited-receptor state, to the closed-duration histogram (a) would not be measurable or (b) could not be assigned to a definite state. However, Tan and Barrantes (1980) have found that fluorescence emission of an antagonist changes upon binding and can be used to study the fast kinetics of antagonist-acetylcholine receptor interactions.

Voltage jumps in the presence of agonist and antagonist lead to relaxations to new levels of agonist-induced current owing to the voltage sensitivity of the open-channel closing rate constant. The presence of a competitive antagonist reduces the amplitude and modifies the rate of the voltage-jump relaxation. For competitive antagonists that bind and unbind rapidly to the receptor, the effective first-order opening rate constant is reduced in proportion to the antagonist concentration and this reduction is kinetically equivalent to a reduction in agonist concentration alone (Gaddum, 1937). On the other hand, an antagonist that binds and unbinds slowly with respect to the duration of the voltage step does not change the voltage-jump relaxation rate constant. Instead, a fraction of the receptor pool is unavailable for activation because antagonist is bound for the duration of the voltage jump (Sigworth, 1980). Competitive antagonists with molecular rate constants between these two extremes will have two or more components to their voltage-jump relaxations.

d-Tubocurarine is a classical competitive antagonist at the nicotinic acetylcholine receptor of many vertebrates, as first suggested by Langley (1905) and later confirmed by Jenkinson (1960) and Adams (1975). At concentrations below 4 μM and at the normal resting potential, curare does not reduce the elementary conductance or change the lifetime of the open channel (Katz & Miledi, 1972). Curare can also bind to the open channel and transiently block the flow of ions through the channel. This local anesthetic effect is important only at hyperpolarized potentials and high d-tubocurarine concentrations (Manalis, 1977; Colquhoun *et al.*, 1979). Therefore, when studying competitive antagonists the experimenter must employ conditions that minimize the local anesthetic effect of the compound. The molecular rate constants for curare binding to closed channels have not been measured accurately. Del Castillo & Katz (1957)

reported on an experiment designed to measure the rate at which curare unbinds from the receptor. While monitoring a frog muscle fiber's response to an iontophoretic pulse of agonist versus time after an iontophoretic pulse of curare, they observed that the inhibition by curare decayed on a time scale of several seconds and suggested that this recovery represented the molecular rate of dissociation of the curare-receptor complex, although they noted that other interpretations were possible. Voltage-jump experiments in the presence of an agonist and curare, however, do not reveal a component with this time scale. In the presence of curare, the rate of the voltage-jump relaxation is slowed just as if the agonist concentration were reduced by a factor $1/(1+[I]/K_i)$. (where [I] is the curare concentration and K_i is the equilibrium binding constant of curare for the receptor, Jenkinson, 1960). This result implies that d-tubocurarine can associate to and dissociate from the receptor many times during the lifetime of the open channel. More recent experiments (Colquhoun *et al.*, 1979; Katz & Miledi, 1978) reveal that the kinetics of curare association and dissociation are at least 10 times faster than acetylcholine channel relaxation kinetics. The paradox of curare's slow recovery kinetics seen in earlier experiments (Del Castillo & Katz, 1957) may be resolved by recognizing that the apparent rate of diffusion of a drug out of the synaptic cleft will be slowed by rebinding to its receptors; macroscopic kinetic measurements will, therefore, be inaccurate. The high density of ACh receptors in the cleft and the high affinity of curare for its receptor combine to slow the diffusion of curare into or out of the cleft by a factor of up to 1000. This 'buffering' effect on curare within the synaptic cleft has been studied by Armstrong and Lester (1979). They concluded that the molecular dissociation rate constant of d-tubocurarine from the receptor is at least 10/s and more likely to be 1000/s. The buffering will slow the recovery by 600-fold yielding a macroscopic dissociation rate constant between 0.02/s and

2/s. This range includes the rates found by Del Castillo and Katz.

Although many other competitive antagonists of the nicotinic acetylcholine receptor are known, studies of their molecular mechanisms of action are similarly complicated. 2,2'-*bis*-[α-(trimethylammonium)methyl]azobenzene (2BQ), a competitive antagonist of the acetylcholine receptors of *Electrophorus electricus* electroplaques (Lester *et al.*, 1980b), exists in two isomeric forms, *cis* and *trans*, and is photoisomerizable (Krouse *et al.*, 1982). It has been demonstrated that *cis* and *trans* isomers can be interconverted by selection of the appropriate wavelength of irradiation; at 327 nm the conversion is to the predominate *cis* isomer (85% *cis* at photoequilibrium) while at 450 nm the photostationary state contains only 20% of the *cis* isomer (80% *trans*). The *cis* and *trans* isomers have differing receptor binding affinities with the *cis* isomer ~ 3 fold more potent than the *trans* isomer. These properties enable step changes to be made in the antagonist activity of solutions of 2BQ by changing the mole-fractions of *cis*- and *trans*-2BQ in response to light flashes.

Because the binding of a competitive antagonist is not voltage sensitive, only concentration jumps can directly perturb the antagonist-receptor interaction. Bath application or iontophoresis cannot produce a step change in the antagonist concentration because of the slow buffered diffusion into the cleft. The change must occur uniformly over the entire synaptic region and rapidly with respect to the competitive antagonist binding if each antagonist binding reaction is to have the same binding rate. The light-flash technique pioneered by Lester and Chang (1977) is more appropriate for the study of competitive antagonist action. The concentration of one isomer of a photoisomerizable drug can be changed in 1 ms using flashlamps (much less with a pulsed laser, Sheridan & Lester, 1982). Buffered diffusion within the synaptic

cleft is minimized with the light-flash technique. The cell is equilibrated in the test solution before each flash, therefore many of the buffering sites (receptors, esterase, etc.) are already bound with competitive antagonist. In addition a light-flash results in the release of some of the bound antagonist into the cleft. This redistribution of antagonist molecules reduces the effect of buffered diffusion on the relaxation rate constants (Nass *et al.*, 1978). Thus, the light-flash technique was used to produce a step change in the antagonist concentration within the cleft. The change in the antagonist concentration induced a change in the number of open channels and the relaxation to a new equilibrium can be measured using a voltage-clamp circuit. Numerical simulations of antagonist concentration jumps versus voltage jumps suggest that the light-flash technique can measure antagonist rate constants that are 5 times larger than those measurable with the voltage jump-technique. The purpose of this study was to use the greater sensitivity of the light-flash technique to measure the molecular rate constants of a photoisomerizable competitive antagonist of the nicotinic acetylcholine receptor.

METHODS

Giant electric eels, *Electrophorus electricus* (4' in length), obtained from World-Wide Scientific Animals, Apotka, FL 32703, were maintained at room temperature in fresh water aquariums and fed 1-2 goldfish daily. Any diseases were treated with nifurpirinol (0.28 mg/gal.) and tetracycline (25 mg/gal.) obtained from a local tropical fish store.

The photoisomerizable competitive antagonist (2,2'-*bis*-[α-(trimethylammonium)methyl]azobenzene) (2BQ) used in these experiments was obtained from B. F. Erlanger and N. H. Wassermann at Columbia University (Bartels, Wassermann, & Erlanger, 1971). Solutions made from the crystals of 2BQ contained only the pure *trans* isomer of 2BQ. The pure *cis* isomer was obtained by exposing a concentrated solution (2 mM) of 2BQ to ultraviolet (UV) light, followed by high-pressure liquid chromatography to separate the *cis* and *trans* isomers (Nerbonne *et al.*, 1983). Tetrodotoxin and the agonists (acetylcholine, carbachol, and suberyldicholine) were purchased from Sigma Chemical Co., St. Louis, MO 63172.

Preparation

To obtain single, isolated electroplaques, a 1" thick slice was surgically removed from the tail of the *Electrophorus*. After cauterization of the wound, the animals were returned to their tanks and allowed to recover for at least 24 hours prior to further surgery. Individual cells from the organ of Sachs were dissected free from the connective tissue under a compound microscope and

stored in glucose-eel Ringer. The Ringer had the following composition:

NaCl	160 mM,
KCl	2.5 mM,
$MgCl_2$	2.0 mM,
$CaCl_2$	2.0 mM,
Glucose	6.0 mM,
Na-Hepes	10 mM,

buffered to pH 7.2-7.4. Test solutions contained Ba^{++} (3 mM) to block the voltage sensitive inward rectifier (K^+ current) and tetrodotoxin (1 μM) to eliminate the fast inward Na^+ current.

For recordings, single, isolated electroplaques were mounted on a nylon grid between two thin Mylar sheets and the Mylar sheets were clamped together with Plexiglas blocks and secured to the cooling block (Fig. 1). The innervated face was exposed to pool A (volume 1 ml) through a circular hole (diameter 0.7 mm) in the top Mylar sheet. The noninnervated face was exposed to pool B (volume 20 ml) through a circular hole (diameter 5 mm) in the bottom sheet of Mylar (Fig. 1). The temperature of pool B was controlled by regulating the temperature of the cooling block via a circulating water bath. Pool B was used as a heat sink or heat source for the cells, the mounting chamber, and pool A. Test solutions were, in addition, heated or cooled prior to perfusion into pool A. Experiments were conducted between 5° and 30°C, and in all cases, the temperature was maintained to within ± 1°C, as measured by a thermistor in pool A.

Current was passed between chlorided Ag or Pt electrodes in pools A and B and measured with a virtual-ground circuit connected to the electrode in pool A. The potential across the electroplaque and innervated face was measured with three glass microelectrodes: extracellular electrodes in pool A and in pool B (<1 MΩ), filled with 1 M NaCl, straddled the electroplaque and measured the potential across the cell (V_a-V_b); the third intracellular electrode (~10 MΩ), filled with 3 M KCL, measured the resting potential of the

Figure 1a

Schematic View of the Apparatus

Light from a xenon short-arc flash tube, placed at one focus of an ellipsoidal mirror, was passed through a 290 nm long-pass filter to remove light of wavelength less than 290 nm. The light was then filtered, when necessary, and focussed with a quartz lens onto the electroplaque. The glass microelectrodes in pool A and pool B measure the voltage of these two pools of solution (V_a and V_b). The intracellular electrode measured the resting potential of the electroplaque (V_i). The Ag or Pt electrode in pool B passed the current from the voltage-clamp circuit. The second Ag or Pt electrode, in pool A, passed the current required to maintain pool A at zero potential. The Plexiglas cooling block cooled the solution in pool B which in turn cooled the electroplaque and pool A. A thermistor in pool A measured the temperature of the solution bathing the preparation.

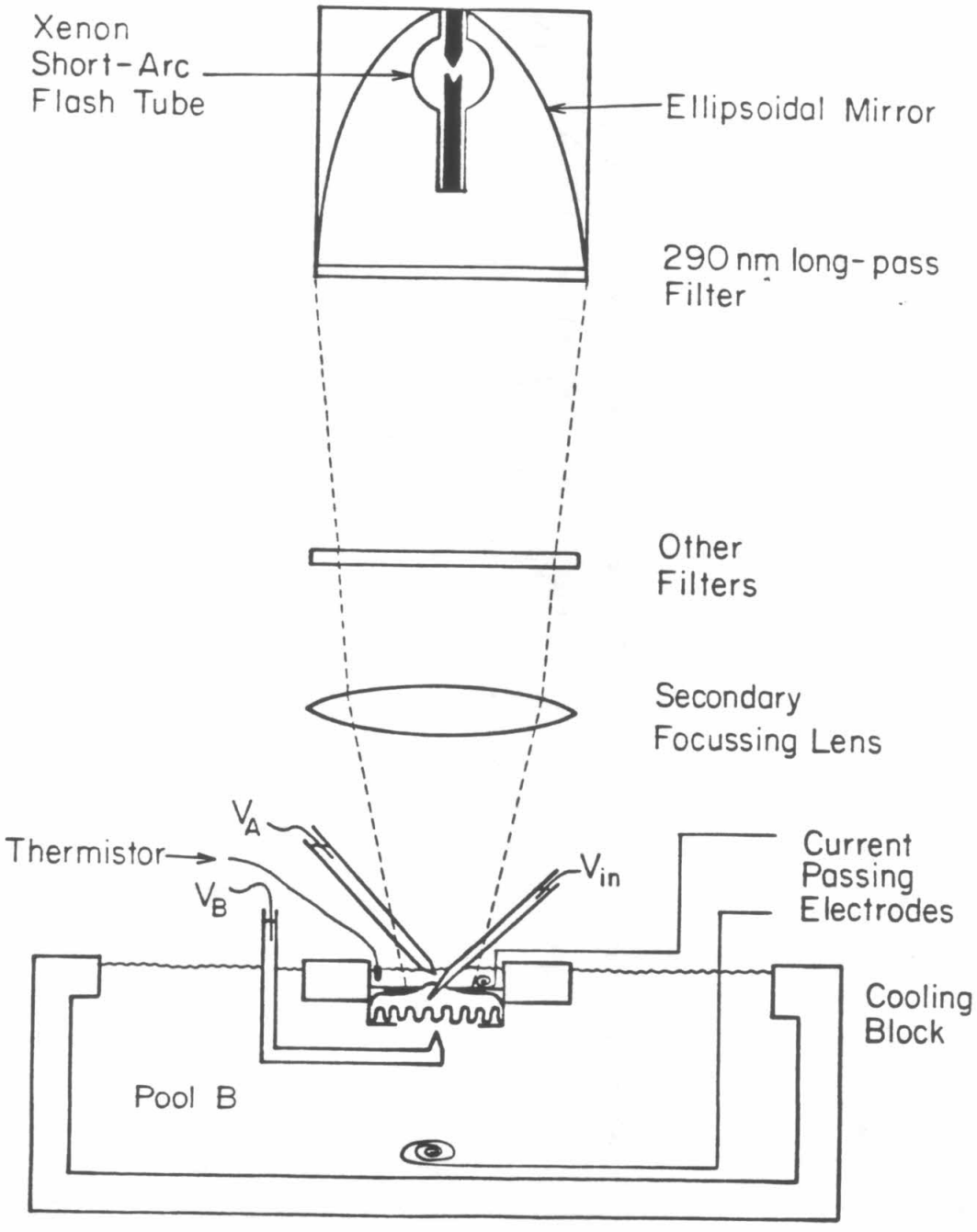
Xenon
Short-Arc
Flash Tube
Ellipsoidal Mirror
290 nm long-pass
Filter
Other
Filters
Secondary
Focussing Lens
V_A
Thermistor
V_B
V_{in}
Current
Passing
Electrodes
Cooling
Block
Pool B

Figure 1b

Exploded View of Electroplaque and Clamping Blocks

The electroplaque was supported on a nylon grid and placed between two thin Mylar sheets. The electroplaque was exposed to pool A and pool B through a 0.7 mm diameter hole in the top Mylar sheet and a 5 mm diameter hole in the bottom Mylar sheet, respectively. Plexiglas blocks were used to clamp the electroplaque holder together. The top Plexiglas block contained a hole which formed pool A. The whole holder was attached to the cooling block. Vaseline was used to provide an electrical seal around the electroplaque so that current flow from pool B to pool A passed through only the electroplaque.

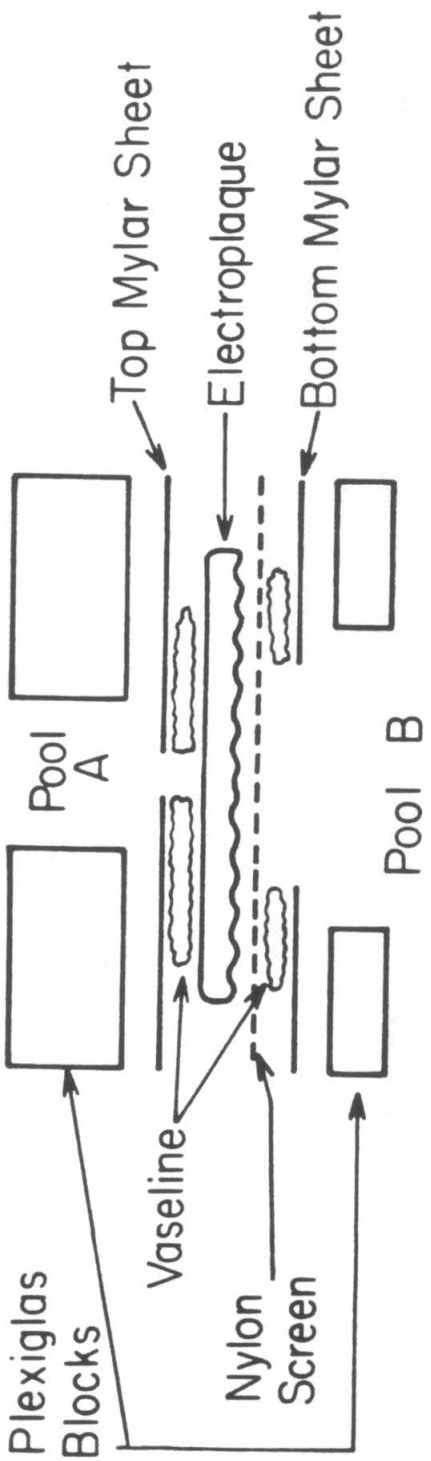
Top Mylar Sheet
Electroplaque
Bottom Mylar Sheet
Pool A
Pool B
Plexiglas Blocks
Vaseline
Nylon Screen

electroplaque (V_i). The two extracellular microelectrodes were carefully positioned above and below the area of membrane exposed by the openings in the Mylar sheets (less than 1 mm vertical separation) in pool A and B, respectively (Figure 1a).

Electronics

The voltage across the innervated face (V_i) was measured by the intracellular electrode with the feedback loop open, 24 msec before each episode, and subtracted from the computer generated voltage-clamp level (V_c) so that the command voltage (V_1) delivered to the voltage-clamp circuit results in the same trans-membrane voltage (V) regardless of the resting potential of the electroplaque.

$$V_1 = V_c - V_i$$

When the feedback loop was closed the circuit passed the appropriate amount of current through the Ag or Pt electrodes so that V_1 = the estimated voltage (V) across the innervated face. (The low resistance of the microelectrodes in pool A and B minimized the RC time constant of the voltage measuring circuit.) Analog circuits computed the membrane potential (V) for input to the feedback circuit:

$$V = (V_b - V_a) - IR_s - V_{ni} - (V_b - V_a)_o$$

$(V_b - V_a)$ is the voltage difference between pool A and pool B.

V_{ni} is the IZ drop across the impedance of the noninnervated face (estimated by Sheridan and Lester (1977) at 20% of IR_s).

IR_s is the voltage drop across the Ringer solution between the microelectrodes in pool A and pool B.

$(V_b - V_a)_o$ is voltage difference between pool A and pool B computed before each trial and was adjusted to be zero. Since pool A is connected to a virtual-ground circuit $V_a = 0.IR_s$ was compensated by subtraction of a voltage step from V. The amplitude of the step was variable and was adjusted until a step-current pulse, passed between pools B and A produced only an exponential charging curve as

Figure 2

Voltage-Clamp Circuit Diagram

The circuit contained eight LF 356A JFET (National Semiconductor) input operational amplifiers. Each amplifier had a 25K potentiometer connected between pin 1 and 5 with the wiper arm of the potentiometer connected to +12 V. The computer controlled the JFET switches (AHO133, National Semiconductor). There were panel-mounted null adjusts for the computer generated command voltage and for the voltage difference between pool A and pool B. Four other panel-mounted potentiometers controlled: the series resistance (R_S) compensation, the high-frequency gain, the low-frequency gain, and the output resistance. When the feedback loop was closed the clamp passed current through the current-passing Ag or Pt electrode until the voltage measured across the cell(V_B-V_A), corrected to yield the voltage across the innervated face (V), equalled the computer generated command voltage (V_1) (the potential at summing junction A equalled zero). The measured voltage-clamp current contained both the agonist-induced current and the passive (capacitive and ohmic) currents.

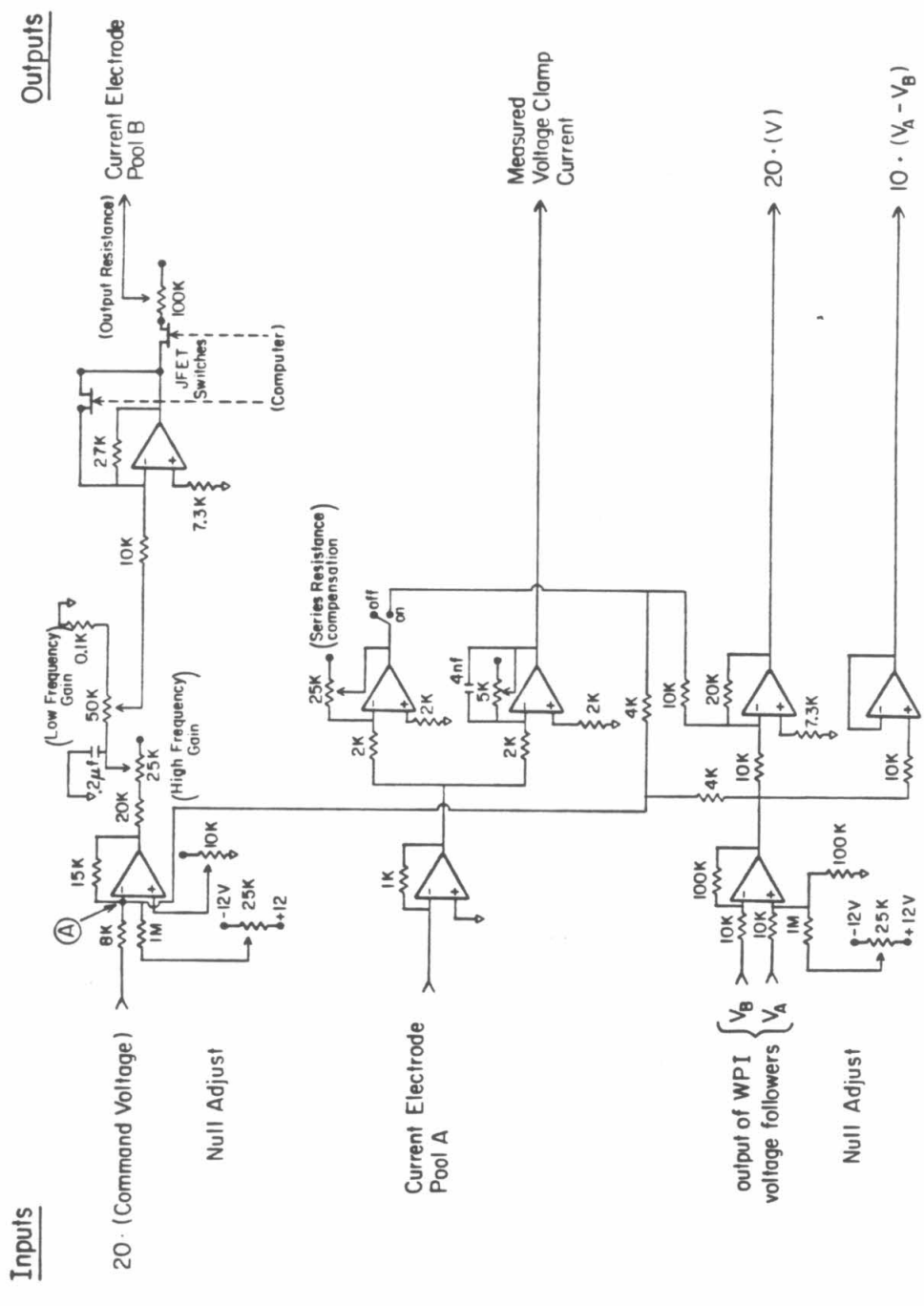
Inputs
Outputs
20 · (Command Voltage)
Null Adjust
Current Electrode Pool A
output of WPI voltage followers
Null Adjust
Current Electrode Pool B
(Output Resistance)
JFET Switches
(Computer)
Measured Voltage Clamp Current
20 · (V)
10 · (VA - VB)
(Low Frequency Gain)
(High Frequency Gain)
(Series Resistance compensation)
off
on
15K
8K
1M
20K
.2μf
50K
0.1K
25K
10K
-12V
25K
+12
1K
27K
7.3K
100K
2K
4nf
5K
4K
100K
10K
1M
-12V
25K
+12V

measured by the microelectrodes in pool A and B. Because complete compensation resulted in oscillations of the voltage-clamp circuit, IR_s could only be 90% compensated experimentally.

Measurement of Agonist-Induced Currents

After an electroplaque was mounted in the experimental chamber, Ringer containing Ba^{++} and TTX was added to pool A, the electrodes were positioned, and the voltage clamp zeroed. The speed of the clamp was then optimized by adjusting the low-frequency gain, the high-frequency gain, and the series resistance compensation.

In a typical experiment, 5-11 applications of agonist and numerous washes were completed on a single electroplaque. The first two agonist applications (not recorded) were performed to check the viability of the preparation, to insure the reproducibility of the response of the cell to agonist exposure, and to provide a measure of the time of diffusion of agonist molecules from pool A to receptors. In subsequent agonist applications (trials), voltage-jump episodes were recorded after the estimated diffusion time had elapsed. After each agonist trial, the solution in pool A was exchanged for Ringer three times over a period of 5 min. At the end of the wash cycles, no agonist-induced currents were measured in voltage-jump episodes. For measurements of agonist-induced currents in the presence of 2BQ, the innervated face of the electroplaque was preincubated with 2BQ alone for 5-10 min. After trials in agonist and 2BQ, cells were washed several times with Ringer over approximately 15 min to insure that 2BQ had been completely removed from pool A. All experiments in the presence of 2BQ were preceded and followed by trials in which only agonist was present.

Experiments were controlled by a Data General Nova 2/10 computer. The

computer initiated each voltage-jump episode: set the level and duration of the voltage step; controlled the frequency of voltage-jump episodes in each trial; and triggered the light flash (when applicable). A typical voltage-jump trial consisted of 3-8 episodes at intervals of 1-10 sec and each episode had a duration of 15-300 ms.

Two methods were used to measure the passive membrane currents. In the first method depolarizing and/or hyperpolarizing voltage-jump episodes in the absence of agonist were recorded. In the second method, episodes were recorded only in the presence of agonist. Because electroplaque acetylcholine channels do not pass net outward current, several small depolarizing voltage-jump episodes with agonist were summed to determine capacitive and ohmic currents. These two methods for measuring the passive currents were employed during experiments and the results compared. In the data reported the two methods yielded results that agreed to within 5%.

Voltage-jump trials in the presence of agonist alter the agonist-receptor complex and, therefore, the amplitude and kinetics of agonist-induced currents. Experiments employing this methodology, then, probe the nature of the agonist-receptor interactions and permit determination of the factors (i.e., voltage, agonist concentration, temperature, etc.) which affect the properties of the measured currents. Similarly, voltage-jump experiments conducted in the presence of 2BQ evaluate its effect on agonist-receptor interactions. Because 2BQ has the additional property of photoisomerization, the combination of light-flash and voltage-jump experiments provide detailed mechanistic information on the binding and unbinding of 2BQ to receptors.

Photochemistry

The optical arrangement used in these experiments is similar to that previously described (Nass, Lester & Krouse, 1978). There were two

improvements: (a) the xenon short-arc flash tube was placed at one focus of a polished ellipsoidal mirror rather than in the lamp housing used previously; and (b) the capacitor bank had a capacitance of 2100 μF and was charged to 450 V (Nargeot *et al.*, 1983). The flash rises to a peak in <100 μs and falls with a time constant of 0.5 μs. This arrangement resulted in an increase (a factor of 5 for UV light) in the amount of light delivered to the preparation per flash over that obtained with the apparatus used previously (Nass, Lester & Krouse, 1978).

Light emitted from the lamp was filtered to remove λ<290 nm (Schott WG 295) and focussed on the preparation with a quartz lens (focal length 75 mm, numerical aperture 0.16). In this configuration visible-light flashes were obtained. A UV-only filter (Schott UG-11) was placed in the light path when ultraviolet flashes were needed. Other filters, when necessary, were placed in the light path between the ellipsoid mirror and the focussing lens.

The crystalline 2BQ used in these experiments was obtained as the pure *trans* isomer. In solution, *cis*-2BQ is formed upon irradiation of the *trans* isomer as the two isomers interconvert in the presence of light. The thermal isomerization of *cis*→*trans* in solution is slow ($t_{1/2}$ = 1 hr at 50°C). The percent of each isomer in a solution depends on the wavelength (λ) of irradiation and was calculated from the optical spectra of the solutions using Beer's law. The absorption spectra of pure *cis*- and *trans*-2BQ are shown with the structure of 2BQ in Fig. 3. The optical density (OD) of the solution at 327 nm (absorptance maximum of *trans*-2BQ) divided by the OD at 281 nm (the isosbestic point) provides a concentration independent measure of the isomeric composition.

$$\text{mole-fraction } trans = \frac{[(\text{OD } 327/281)_x - (\text{OD } 327/281)_{cis}]}{[(\text{OD } 327/281)_{trans} - (\text{OD } 327/281)_{cis}]}$$

Figure 3

The absorption spectra of pure *trans* (solid line) and pure *cis* (dashed line) 2BQ. The absorption maximum of the *trans* isomer is 327 nm. 2BQ can isomerize between the *cis* and *trans* isomers upon absorbing a photon ($h\nu$). Irradiation with any wavelength near 327 nm will produce a predominant *cis* photostationary state. Conversely, at wavelengths greater than 400 nm the photostationary state is predominant *trans* isomer. An isosbestic point at 287 nm was used in the computation of the mole-fraction of *cis* in solutions of 2BQ. The structure of 2BQ is also shown.

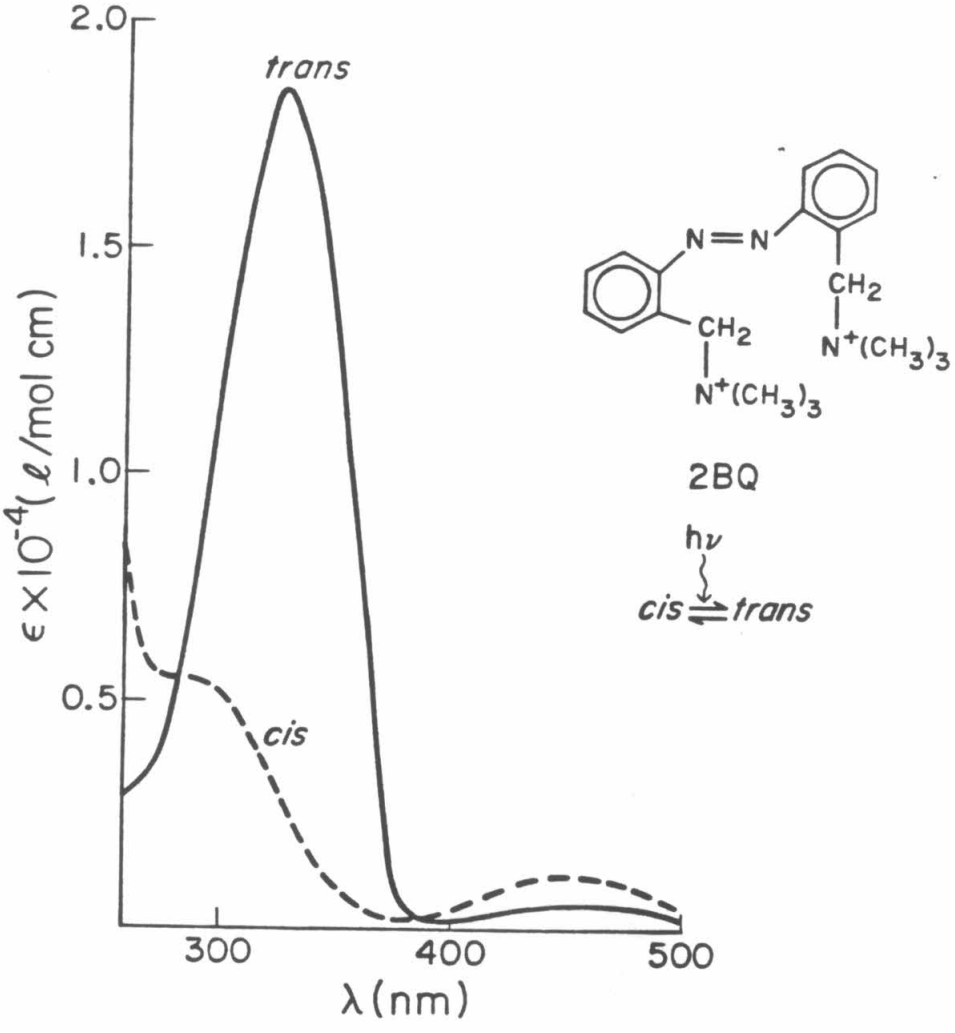
2.0
1.5
1.0
0.5
trans
cis
$\epsilon \times 10^{-4}$ (ℓ/mol cm)
300
400
500
λ (nm)
N=N
CH2
N+(CH3)3
CH2
N+(CH3)3
2BQ
hν
cis ⇌ trans

UV irradiation (300 <λ<360 nm) yields 85% *cis* and 15% *cis* and *trans* photostationary state, CPSS). Visible irradiation (400 <λ<500 nm) yields 20% *cis* and 80% *trans* (*trans* photostationary state, TPSS). With the optical arrangement employed here a single visible flash delivered to a solution of 100% *cis*-2BQ yielded a solution containing 76% *trans* and 24% *cis*-2BQ (95% of the way to the *trans* photostationary state). A single UV-only flash delivered to a solution of 100% *trans*-2BQ produced a solution containing 38% *cis* and 62% *trans* (45% of the way to the *cis* photostationary state).

Previously the photoisomerization potencies, k_t and k_c have been described (Nass *et al.*, 1978; Sheridan & Lester, 1982). The two potencies are defined by the following statements: (a) the *cis* photostationary state has the mole-fraction *cis* = $k_t/(k_t + k_c)$ and (b) the approach to this state is described by $\exp[-(k_t + k_c)\, n]$, where n is the number of flashes. Therefore, k_c and k_t are pseudo-rate constants with the units of flash^{-1}. $k_t + k_c$ equals 0.6 (-In (1-.45)) and 3.0 (-In (1-.95)) for the UV and visible flash, respectively. A calculation of k_c and k_t can be found in the Appendix.

Data Analysis

Digitized current records from each voltage-jump trial were stored during the experiments on floppy disks. For analyses, control trials were subtracted from the trials in the presence of agonist and the resultant agonist-induced currents displayed on an X-Y scope. The agonist-induced currents were digitally filtered (single-pole recursive filter) as necessary. The final 10% of the episode or maximum of the agonist-induced current is assumed to be the steady-state value of the agonist-induced current and, when present, a sloping base line was fit with a straight line and subtracted from the agonist-induced current to provide a better estimate of the steady-state amplitude. The steady-state values were plotted as the responses in dose-response curves and used to

determine the equilibrium binding constant of 2BQ for the receptor.

For determination of the relaxation rate constants, the first few data points (usually less than 1 ms) after the voltage jump or light flash were ignored because of contamination from gating currents, voltage-clamp settling time, and electrical artifacts produced by the flash lamp. The voltage-jump currents were fit with a single exponential, using a least squares fit to the semilogarithmic plot of the approach to steady state (Fig. 4). The fits were usually truncated when the agonist-induced current was within 5% of the steady-state value. In general, semilog plots of the data could be fit with a straight line and, in these cases, the exact point of truncation had no effect on the measured relaxation rate constant. The time constant (τ) of a relaxation equals the (relaxation rate constant^{-1}).

In cases where two or more components to the relaxation were visible, in the presence of 2BQ, two different methods were used to estimate the rate constants. The first method assumes that the relaxation is the sum of two exponentials and these two exponentials, with their corresponding amplitudes, were fit to the relaxation using the method of least squares. This method gave the amplitude and rate constants for both components and was used mainly for the light-flash relaxations. One of the rate constants measured in a light-flash relaxation should reflect 2BQ binding and was the component of interest in these experiments. Alternatively, in the second method, a time span is chosen where one of the components dominates the waveform, and a single exponential is fit to this time span. This method determines only one relaxation rate constant but in many cases a second time span can be chosen to determine the second relaxation rate constant. Where the two methods could be applied to the same relaxation, the relaxation rate constants agree within 10%.

RESULTS

Voltage-Jump Experiments

Equilibrium Measurements

Voltage jumps from +60 to -150 mV (voltage across innervated face, v) produced relaxations in the presence of agonist (carbachol 0.02-1 mM, acetylcholine 5-40 μM, and suberyldicholine 0.5-10 μM) (Fig. 4). From experiments such as these the steady-state agonist-induced conductances were measured as a function of voltage, agonist concentration, and nature of the agonist (Sheridan & Lester, 1977; Takeuchi & Takeuchi, 1960; Adams, 1975). Steady-state conductances increased with increasing agonist concentration and with hyperpolarization (measured over the range -60 to -150 mV). Similar voltage-jump experiments were performed in the presence of agonist and 2BQ (0.1-3.0 μM) (Fig. 4a). In these experiments, the agonist concentration was increased (1.3-11 fold) in order to obtain the same steady-state conductance levels measured in the absence of 2BQ (Fig. 4).

Steady-state conductances (response) were measured at several agonist concentrations (dose) in the presence and absence of varying concentrations of 2BQ and from these data abbreviated log-dose response curves were constructed (Fig. 5). When *trans*-2BQ was present at concentrations less than 4.0 μM dose-response curves were shifted to higher agonist concentrations with no change in slope. Below 3 μM, 2BQ log-dose response curves in the presence of agonist alone and agonist and 2BQ approached the same maximum agonist-induced current at high agonist concentrations (Fig. 6). These results demonstrate that 2BQ behaves as a competitive antagonist at the nicotinic acetylcholine receptor of

Figure 4

The three traces show the agonist-induced current before and after a voltage jump from +60 mV to -150 mV at 6°C. The current approached the steady-state value exponentially. The semilog plot of all three traces is shown above the current traces. The slope of these lines provided a measure of the relaxation rate constant of each trace. The time constants (τ = 1/relaxation rate constant) for all three traces are shown. The traces obtained in 3 μM suberyldicholine (b), 10 μM suberyldicholine (c), and in the additional presence of 2 μM of the *trans* photostationary state of 2BQ (a). The amplitudes of trace a and trace b are equal; however, the time constants for trace b and trace c are the same.

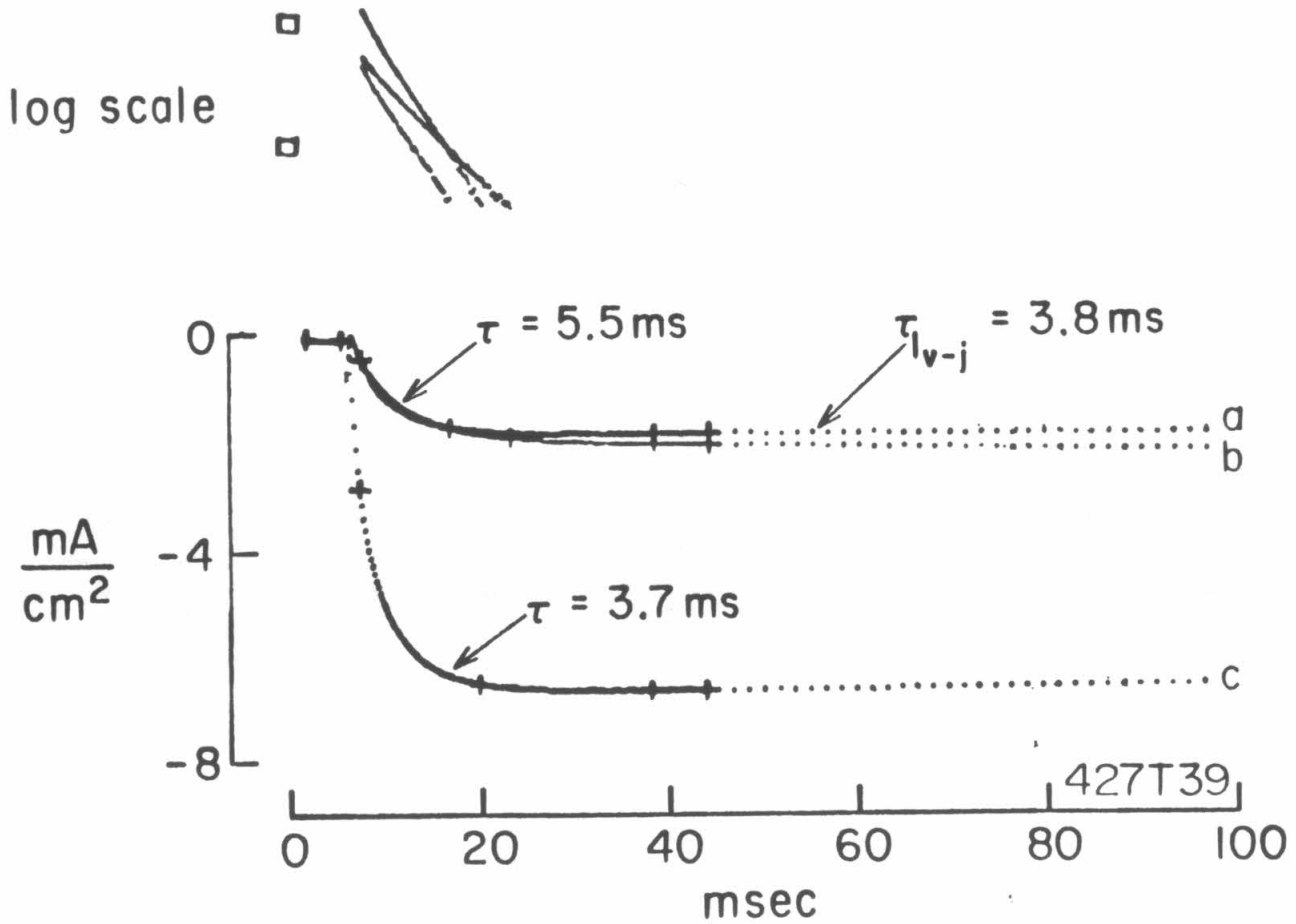
log scale
0
-4
-8
mA
cm²
τ = 5.5 ms
τ I_V-j = 3.8 ms
τ = 3.7 ms
a
b
c
427T39
0
20
40
60
80
100
msec

Figure 5

Inhibition of agonist-induced currents by the *trans* photostationary state of 2BQ. Responses are shown for carbachol alone (o) and in the additional presence of varying concentrations of the *trans* photostationary state of 2BQ. The dose-response curves are shifted to higher agonist concentration with no change in slope as the 2BQ concentration was increased from 0 to 4.0 μM. Above 4.0 μM the parallel nature of the shift was not maintained. The experiments were performed at a membrane potential (v) of -120 mV and 20°C. Error bars give SE of the agonist-induced current measurements (4 cells).

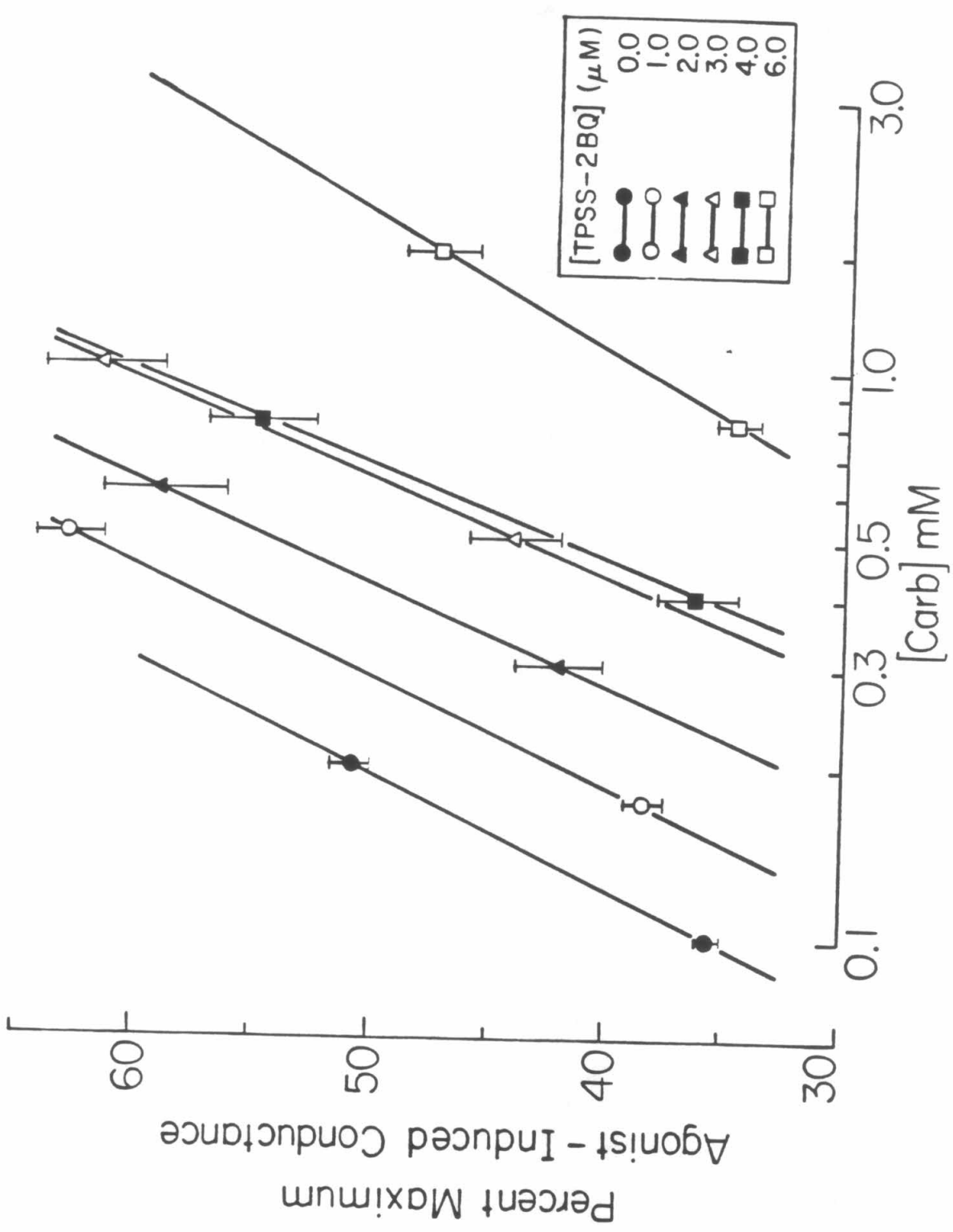
Percent Maximum
Agonist - Induced Conductance
60
50
40
30
0.1
0.3
0.5
1.0
3.0
[Carb] mM
[TPSS-2BQ] (μM)
0.0
1.0
2.0
3.0
4.0
6.0

Figure 6

The maximum agonist-induced current in 500 μM Carb (solid line) and in the additional presence of 0.5 μM of the *cis* photostationary state of 2BQ (dotted line). The upper two curves were taken at -175 mV and the lower two curves at -85 mV. All data were taken at 6°C. The maximum measured response of the cell was 15 mA/cm^2. This value decreased with subsequent agonist applications. The average maximum agonist-induced currents in the presence of Carb alone were 11.6 ± 2.0 mA/cm^2 (-175 mV) and 5.0 ± .8 mA/cm^2 (-85 mV) and in the additional presence of 0.5 μM CPSS 2BQ, 10.4 ± 1.7 mA/cm^2 (-175 mV) and 3.9 ± .6 mA/cm^2 (-85 mV). The values measured at the same voltage were identical within the standard error of the means.

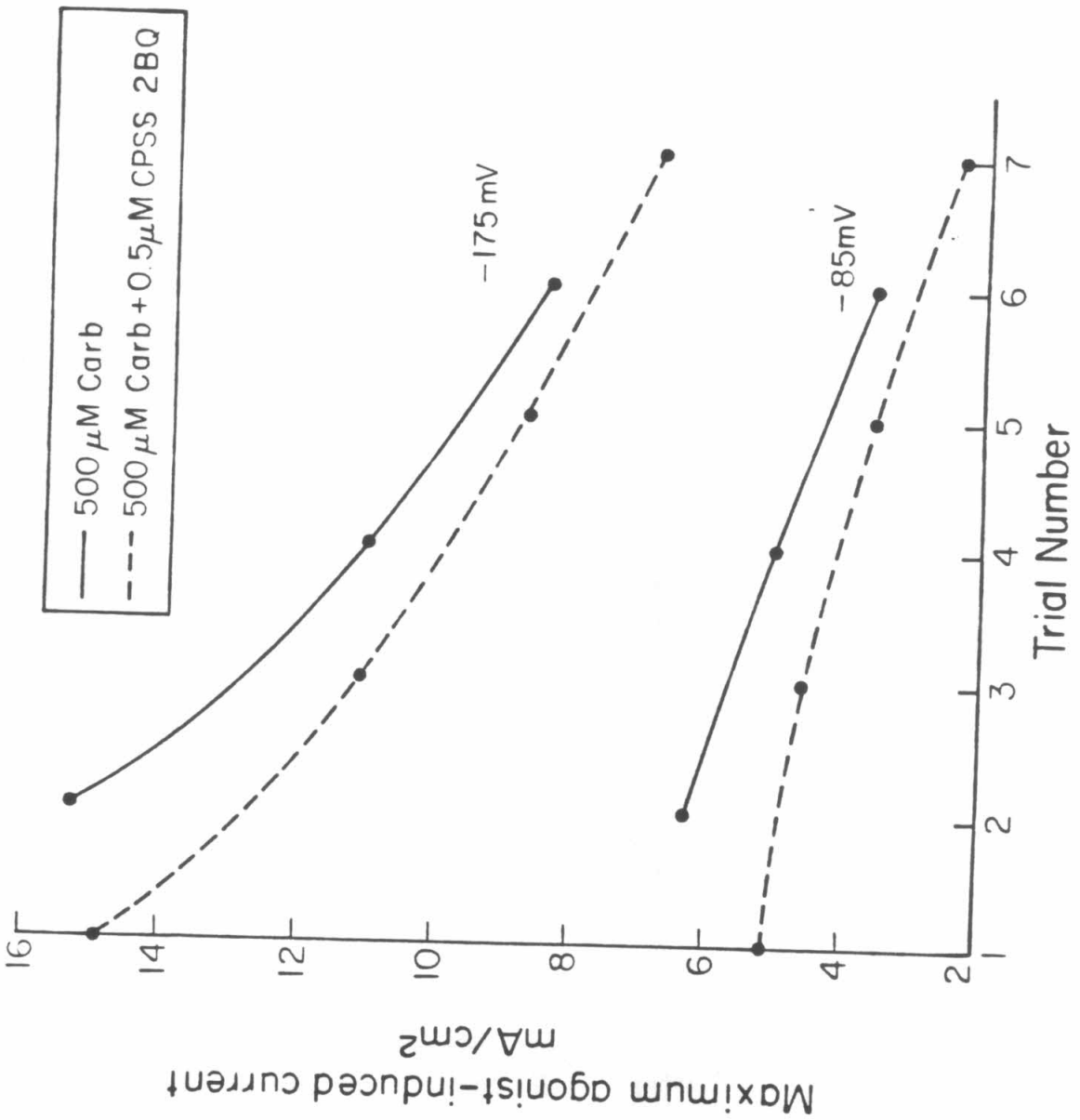
500 μM Carb
500 μM Carb + 0.5 μM CPSS 2BQ
−175 mV
−85mV
Maximum agonist-induced current
mA/cm2
Trial Number
16
14
12
10
8
6
4
2
1
2
3
4
5
6
7

the *Electrophorus* electroplaque. Above this concentration there was a possible local anesthetic effect of *trans*-2BQ which will be discussed later.

The magnitude of the parallel shift in the log-dose response curve was measured as a function of the concentration of 2BQ. The shift (ΔX) was calculated from the horizontal displacement of the curve obtained in the presence of agonist and 2BQ from that with agonist alone:

$$\Delta X = \log([A]_{2BQ}) - \log([A])$$

$$\Delta X = \log([A]_{2BQ}/[A])$$

$$10^{(\Delta X)} = [A]_{2BQ}/[A].$$

The dose ratio, $10^{(\Delta X)}$, therefore can be directly calculated and was a measure of the ratio of the two agonist concentrations which gave the same steady-state response amplitude. When the dose ratio was plotted versus the 2BQ concentration (Fig. 7) the data points fell on a straight line of the form $[2BQ]/K_i + 1$ (where K_i is the equilibrium binding constant or 2BQ). See Appendix, Equation 3, for a derivation of the form of the dose-ratio plots. A plot of the dose-ratio (A'/A) versus the inhibitor concentration ([I]) should be a straight line with slope $1/K_i$ and a y-axis intercept of (0,1). (A more detailed evaluation of the shape of the dose-ratio plot is found in the Appendix, Fig. 18.) The slope of the line fit through the data provided an estimate of the affinity constant ($1/K_i$) of the *trans*-photostationary state of 2BQ. The calculated slope (1.4/μM) was the same for the three voltages in Fig. 7 and for all voltages in the range tested (-60 mV to -150 mV), implying that the apparent affinity of 2BQ for the receptor is voltage independent.

2BQ consists of two distinct isomers in solution and the measurement of affinity of each isomer was necessary if light-flash relaxations were to be

Figure 7

Dose-ratio plot of data like that in Fig. 5. The dose ratio is the ratio of carbachol concentrations giving equal responses in the presence and absence of the 2BQ. The weighted least-squares line, constrained to go through (0,1), is drawn with a slope of 1.4 and an X-axis intercept of -0.7 μM. Three separate voltages were fit with the same line below 4.0 μM. At 6.0 μM the agonist-induced current is decreased and the dose-ratio increased as the membrane potential is hyperpolarized (possible channel block effect). Error bars give SE of the dose-ratio calculations.

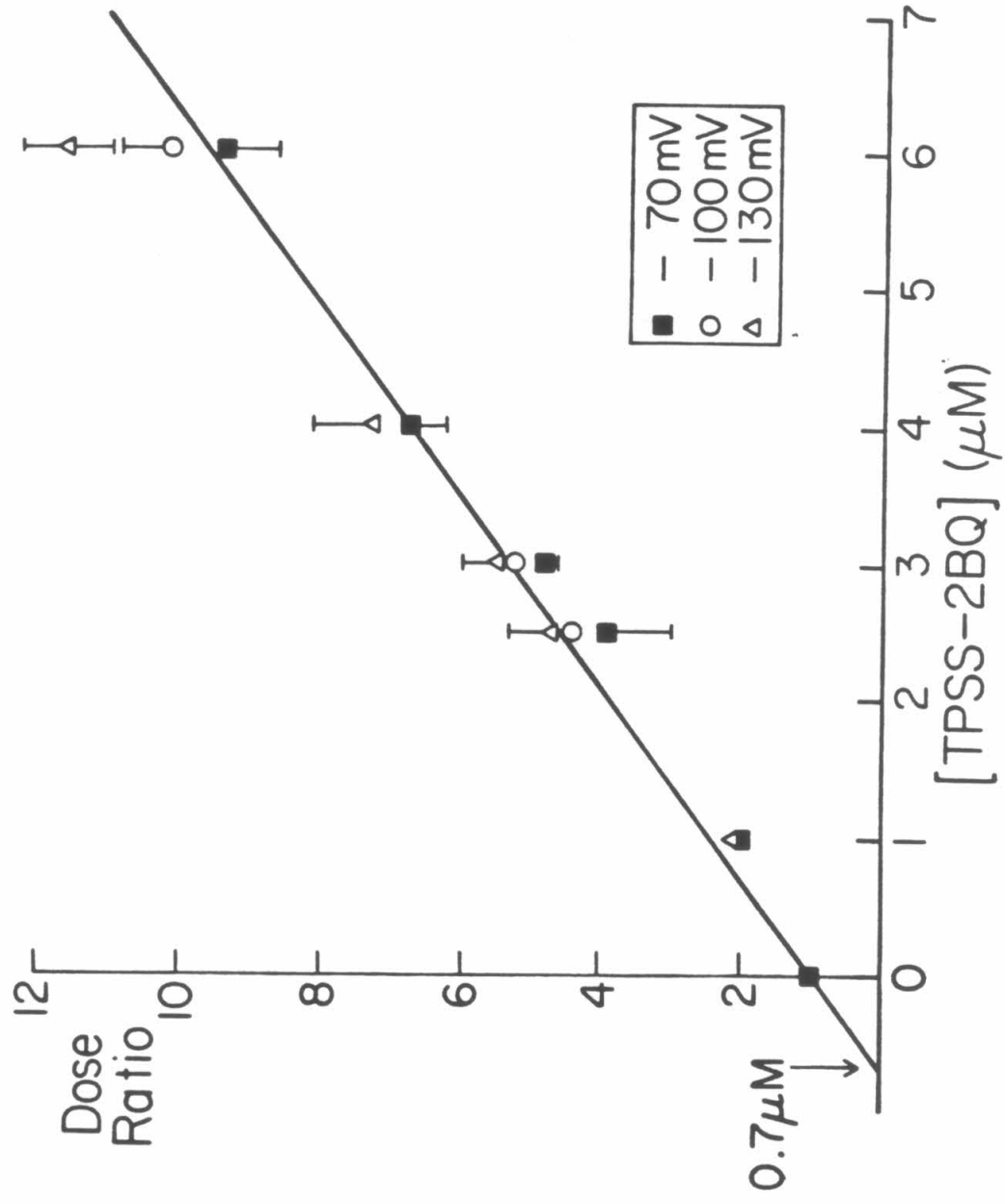
Dose Ratio
12
10
8
6
4
2
0.7μM
0
1
2
3
4
5
6
7
[TPSS-2BQ] (μM)
− 70mV
− 100mV
− 130mV

understood. The apparent affinity ($1/K_i$) of various solutions containing 2BQ which were irradiated with different wavelengths of light were plotted versus the calculated mole-fraction of *cis*-2BQ in the solution (Fig. 8). A straight line fit to the data provided a measure of the equilibrium binding constant for the *trans* (1.0 μM) and *cis* (0.33 μM) isomers of 2BQ.

Kinetic Measurements

Voltage jumps from +60 mV to -150 mV in the presence of any of the three agonists tested produced an increase in agonist-induced current. These relaxations could be fit with single exponentials. As found in previous studies (Sheridan & Lester, 1977) the voltage-jump relaxation rate increased with increasing agonist concentration (same range as for equilibrium studies) and decreased with more negative voltages (-60 mV to -150 mV). Also in agreement with previous results (Lester *et al.*, 1980a), we found that the variation in the relaxation rate constant with temperature was dependent upon the nature of the agonist used. Carbachol, which had the fastest relaxation had the largest (Q_{10}~9) and suberyldicholine, which had the slowest relaxation, had the smallest (Q_{10}~3) variation with temperature (6°-26°C). Voltage jumps obtained in the presence of 2BQ had relaxations with as many as three components. The rate constant of the fastest and largest component (component 1_{V-j}) had the same voltage, agonist concentration, and temperature dependence as that measured in the absence of 2BQ.

Some voltage-jump relaxations had a rate constant for component 1_{V-j} which were smaller than that produced by the agonist alone. Even though this component 1_{V-j} could be fit with a single exponential, it might in fact have been the sum of two or more exponentials. This is possible if one component had the relaxation rate constant of the voltage-jump relaxation in the presence of agonist alone and the second component (component 2_{V-j}) had a much smaller

Figure 8

The affinity (slope of dose-ratio curve) of each solution of 2BQ is plotted versus the mole-fraction of *cis*-2BQ in solution. The pure *trans* and pure *cis* isomers of 2BQ have differing affinities for the receptor (1.0 μM^{-1} and 3.0 μM^{-1}, respectively). The actions of *cis* and *trans* 2BQ on the receptor are independent and the affinity of any solution of 2BQ equals 1 + 2 x (mole-fraction of *cis*-2BQ) μM^{-1}. The error bars represent the SE of the affinity constants determined for 4 cells.

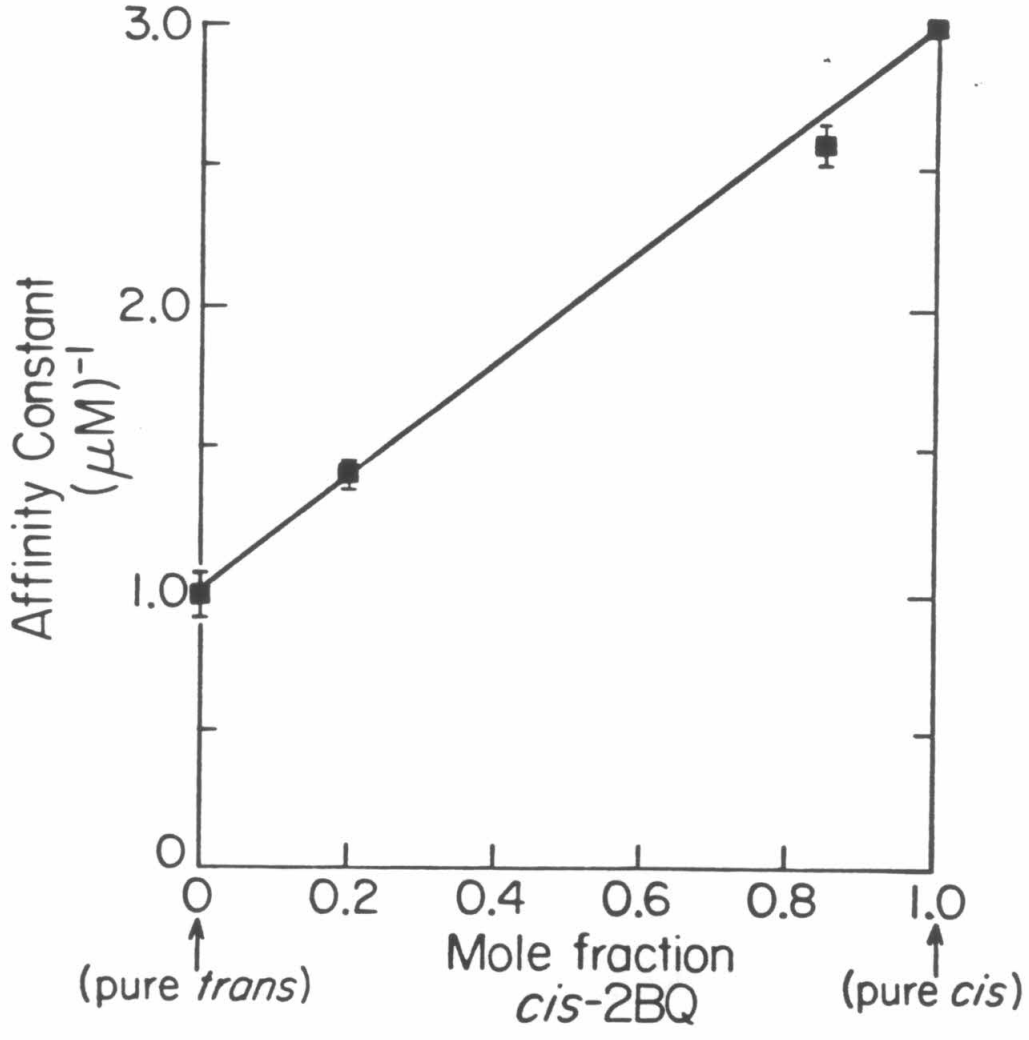
3.0
2.0
1.0
0
Affinity Constant
$(\mu M)^{-1}$
0
0.2
0.4
0.6
0.8
1.0
(pure *trans*)
Mole fraction
cis-2BQ
(pure *cis*)

amplitude (roughly < 10%) than the other faster component. (The theoretical treatment of component 2_{V-j} as the slow dissociation of 2BQ from the receptor can be found in the Appendix.) Since the actual steady-state value could not be measured, due to a third component which obscured component 2_{V-j}, the existence of component 2_{V-j} was not confirmed with voltage-jump relaxations. This third component could be seen as a decrease in current after the agonist-induced current had reached a maximum. The current no longer remained at the maximum agonist-induced current after a voltage jump but declined slowly back toward zero current (Fig. 4). Qualitatively, this component increased in amplitude with increasing agonist or 2BQ concentration or with increasing hyperpolarization. This effect is reminiscent of the local anesthetic effect of d-tubocurarine seen at the neuromuscular junction (Colquhoun *et al.*, 1979). This component was subtracted from the agonist-induced currents, as mentioned in Methods, and its amplitude and relaxation rate constants were not investigated. (See the Appendix, Fig. 20 for a simulation of the local anesthetic effect and its subtraction from the data.)

Visible-Light Flash Relaxations

Light flashes were delivered after the voltage-jump relaxation reached the steady-state. With cells exposed to a photostable agonist alone, the artifact produced by the visible flash lasts less than 500 μs and has an amplitude of less than 0.02 mA/cm^2. Its amplitude is dependent upon the flash intensity and is below the noise of the clamp with the UV filter in place.

The records in Figure 9 show three episodes from a typical visible-light flash experiment on an electroplaque exposed to agonist (carbachol) and the *cis*-photostationary state (CPSS) of 2BQ. Traces 1 and 2 superimpose until halfway through the second episode, when a visible-light flash occurred. The agonist-induced inward current, following the light flash, increased and eventually

Figure 9

Voltage-jump relaxations and a visible-light flash relaxation in the presence of 200 μM Carb and 1.0 μM of the *cis* photostationary state of 2BQ. The first two traces superimpose until halfway through the second trace a visible-light flash occurred. The flash-induced relaxation was fit with the sum of two exponentials. The faster component had a relaxation rate constant similar to that of the subsequent voltage-jump relaxation. All voltage jumps were from +60 to -150 mV at 20°C. The flash intensity was less than in most of the experiments, because the quartz lens was not used.

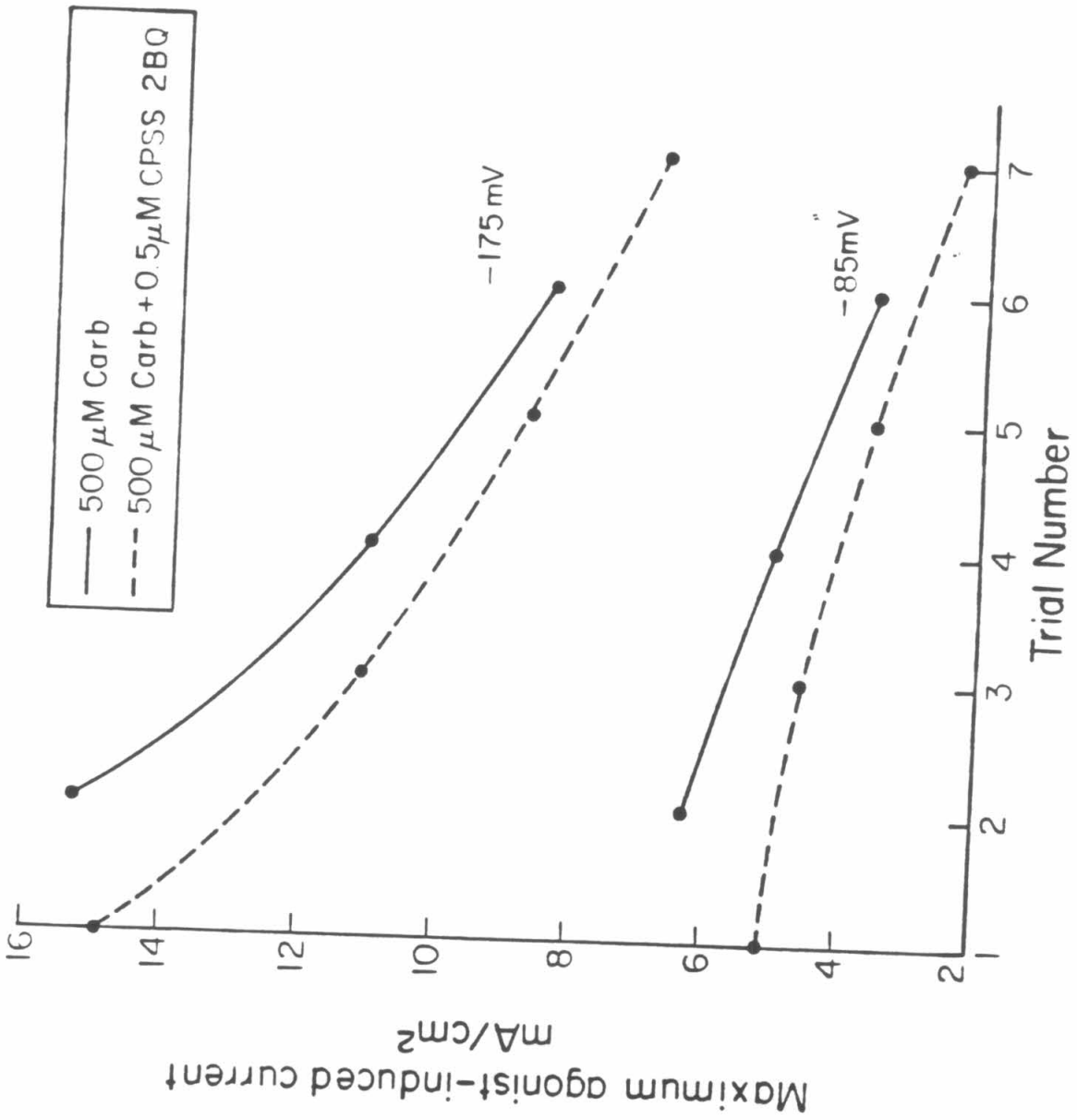
500 μM Carb
500 μM Carb + 0.5μM CPSS 2BQ
-175 mV
-85mV
Maximum agonist-induced current
mA/cm2
Trial Number
16
14
12
10
8
6
4
2
1
2
3
4
5
6
7

reached the steady-state. The increase was fit with the sum of two exponential components (termed component 1_{l-f} and 2_{l-f}) of the same sign. The relative amplitude of (component 2_{l-f})/(component 1_{l-f}) was increased with increasing 2BQ concentration. The amplitude of the light-flash relaxation (component 1_{l-f} + component 2_{l-f}) was determined by the difference in steady-state values for the concentrations of antagonist before and after the flash. This could be estimated from the dose-response curves in Fig. 5 (the amplitude equals the vertical displacement of the curves). The amplitude of any light-flash relaxation was maximized by using a combination of agonist and 2BQ which gave half maximal response (see Appendix for derivation of maximum light response).

The actual sign of component 2_{l-f}, whether an increase or decrease in the current, is dependent upon the initial and final isomeric composition of the 2BQ in which the cell was bathed. As a solution of 2BQ approaches the photostationary state a flash produces less and less change in the net agonist-induced current. At the photostationary state no net change in agonist-induced current is produced but component 1_{l-f} and 2_{l-f} have equal but opposite amplitudes. In Fig. 10 an electroplaque bathed in the *trans*-photostationary state (TPSS) of 2BQ and carbachol was exposed to a visible-light flash. The initial and final states for this relaxation were identical. The voltage-jump relaxation was subtracted from each episode to show the light-induced relaxation. The amplitude of component 1_{l-f} and component 2_{l-f} were equal except that component 2_{l-f} was a decrease back to the original agonist-induced current.

The relaxation rate constants for the two components have been measured under various conditions. The rate constants estimated for component 2_{l-f} were somewhat smaller than those measured for the slower component of the UV-light flash relaxations. This may be due to the fact that the amplitude of component

Figure 10

A visible-light flash relaxation from a cell exposed to 1 mM Carb and 2 μM of the *trans* photostationary state of 2BQ. The initial and final state conditions were identical and there was no change in the net agonist-induced current. The relaxation time constants differ by a factor of 26. Data were taken at -150 mV and 6°C.

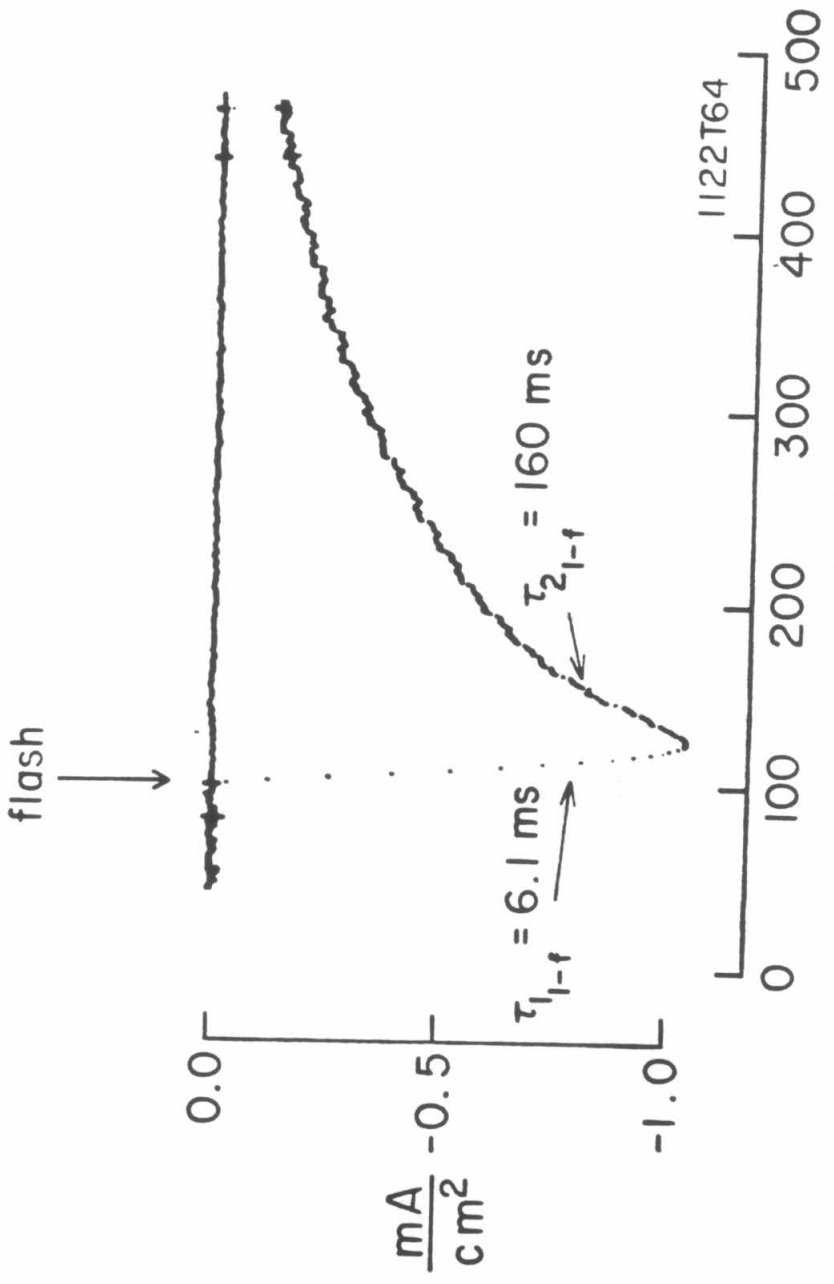
flash
0.0
-0.5
-1.0
mA/cm²
τ1 1-f = 6.1 ms
τ2 1-f = 160 ms
0
100
200
300
400
500
msec
1122T64

2_{l-f} can be quite small and the measure of its rate constant was therefore inaccurate. Therefore, the rate constants for component 2_{l-f} were analyzed in UV-flash experiments.

The rate constants measured for component 1_{l-f} were similar to those measured for the fast increase in agonist-induced current (component 1_{v-j}) after a voltage jump. For the agonists suberyldicholine and acetylcholine, at temperatures below 20°C, the rate constant measured for component 1_{l-f} was identical to that measured for component 1_{v-j} of the subsequent voltage-jump relaxation. At temperatures between 20° and 30°C the rate constant measured for component 1_{l-f} increased less rapidly than that measured for component 1_{v-j}. In the presence of carbachol, at all temperatures between 5° and 30°C, the flash relaxation rate constants were less than those of the succeeding voltage-jump relaxation. At 6°C these rate constants for component 1_{l-f} and component 1_{v-j} generally differed by less than 20% but at 30°C they differed by a factor of 2. It was a general observation that as the flash relaxation rate constant increased to greater than 1 ms^{-1} the measured relaxation rate constant of the flash-induced relaxation was always less than the measured relaxation rate constant of the voltage jump. This discrepancy could not be caused by the settling time of the clamp (100-200 μs), because if the clamp could not accurately measure rates greater than 1 ms^{-1} then both relaxations would be equally affected.

Our analysis of the relaxation rate constants was most useful for conditions where the two exponential components were clearly separable (ACh or Sub at 6°C); in such cases the rate constants of component 1_{l-f} and component 1_{v-j} were independent of 2BQ concentration and increased with increasing agonist concentration. Where carbachol was used as the agonist the relaxation rate constant for component 1_{l-f} and component 1_{v-j} decreased with increasing

2BQ concentration. These results are consistent if the single exponential relaxation in the simultaneous presence of Carb and 2BQ is composed of two relaxations: (a) a fast agonist-receptor interaction (measured directly in Sub and ACh) and (b) a slower antagonist concentration-dependent component.

The voltage-jump relaxation rate constants varied with temperature and with the nature of the agonist. In one series of experiments with voltage jumps in the presence of carbachol, the rate constants increased an average of 8.9 fold for a 10°C increase in temperature ($Q_{10} = 8.9$) between 6° and 26°C. Suberyldicholine has a Q_{10} of 3.4 and acetylcholine had a Q_{10} of 5.5 These experiments were not designed to investigate the differences in temperature sensitivity of the three agonists (see Lester *et al.*, 1980) but rather to exploit these differences to study the mechanism underlying component 1_{l-f} and component 1_{v-j}. As mentioned before the rate constants for component 1_{l-f} were always less than or equal to that of component 1_{v-j}. Table 1 is a tabulation of the ratio of the Q_{10}s of the rate constants for component 1_{v-j} and component 1_{l-f} between 6° and 26°C. Notice that the Q_{10}s of the two components differ by only 17% from the voltage-jump relaxation rate constant Q_{10} for all three agonists. By contrast the Q_{10} for component 2_{l-f} was approximately 3 for all three agonists.

A tabulation of the properties of component 1_{v-j} and component 1_{l-f} (Table 2) is presented to summarize the results of voltage-jump and visible-flash relaxations.

Ultraviolet-light Flash Relaxations

In mostly *trans*-2BQ, UV light increases the mole-fraction *cis* in solution. This increase in the competitive antagonist activity of the solution of 2BQ leads to a conductance decrease. This situation provided the most interesting data. Like the visible-flash relaxations, the UV-light-induced relaxation (Fig. 11) was

Table 1

The three agonists tested had different temperature sensitivities for their relaxation rate constants. The faster component of each relaxation had similar Q_{10}s for each agonist tested. The slower component (component 2_{1-f}) had the same Q_{10} (~3.4) for all three agonists. All data were taken at -150 mV.

Agonist	Voltage-Jump Relaxation Rate Constant (Component I_{v-j}) Q_{10} (6°–26 °C)	Light-Flash Relaxation Rate Constant (Component I_{l-f}) Q_{10} (6°–26 °C)	Ratio
Carb	8.89	6.92	.78
ACh	5.45	4.83	.89
Sub	3.38	2.79	.83

Table 2

Comparison of factors which affect the measured rate constants of the faster increase in agonist-induced current after a perturbation.

	Component I_{v-j} (fast increase in agonist-induced current after a voltage jump)	Component I_{l-f} (fast increase in agonist-induced current after a light flash)
Relaxation Rate Constant	$\propto$ (agonist concentration)	$\propto$ (agonist concentration)
	independent (2BQ concentration)	independent (2BQ concentration)
	$\propto e^{(\text{membrane potential}/85\text{mV})}$	$\propto e^{(\text{membrane potential}/85\text{mV})}$
	Q_{10} agonist dependent	Q_{10} agonist dependent
	relaxation rate constants equal at low temperatures	

Figure 11

A series of three voltage jumps with a UV-flash occurring during the second episode. The first and second traces superimpose until the arrow when a UV-flash occurred. The increased *cis*-2BQ concentration induced a reduction in current to the new steady-state value (third trace). In the upper half of the figure the light flash relaxation has been amplified after the third trace was subtracted from the second. The relaxation rate constants for the voltage jump and light flash differ by a factor of 9. All three traces were taken in 500 μM Carb and 2 μM *trans* photostationary state 2BQ at 6°C.

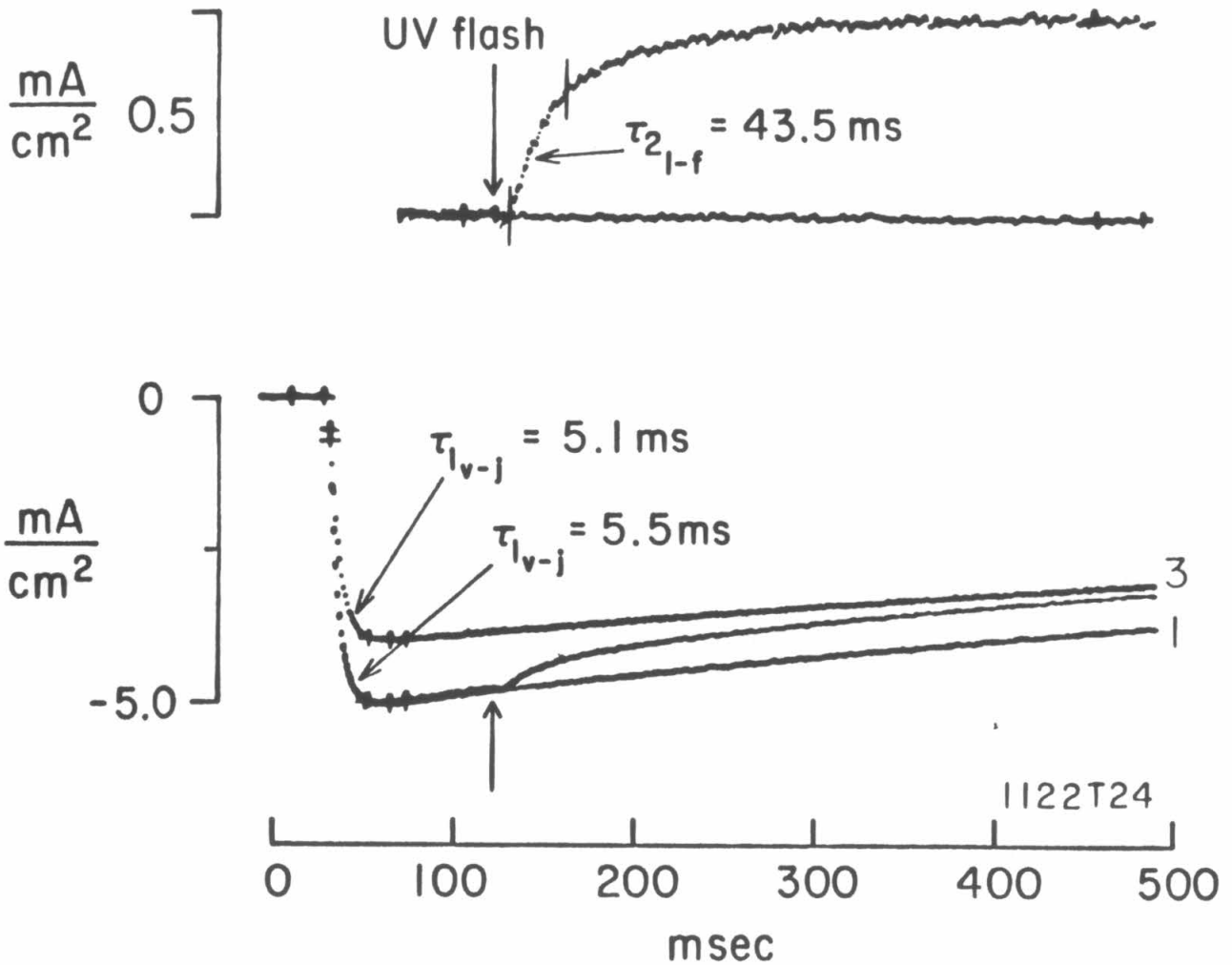
mA/cm²
0.5
UV flash
τ2 I-f = 43.5 ms
0
mA/cm²
-5.0
τ1 V-J = 5.1 ms
τ1 V-J = 5.5ms
3
1
1122T24
0
100
200
300
400
500
msec

composed of two components just as were visible-light-flash relaxations. Component 1_{l-f} in both cases was a fast increase in agonist-induced current. Component 2_{l-f} for UV-only flashes was a slow decrease in agonist-induced current, as opposed to the slow increase seen in many visible-flash relaxations.

The amplitude of component 1_{l-f}, at a constant voltage and receptor activation, depended upon the wavelength of the irradiation and the initial isomeric composition of the 2BQ solution bathing the electroplaque. The relative amplitude of component 1_{l-f} (amplitude component 1_{l-f}/amplitude component 2_{l-f}) increased as the wavelength of irradiation increased from 320 to 450 nm (Fig. 12). In fact the amplitude of component 1_{l-f} increased as the unidirectional flux from *cis→trans* increased (see Appendix for calculation of unidirectional fluxes). Table 3 lists the wavelength of the irradiation and the relative amplitude of component 1_{l-f} for the different filters used. At wavelengths > 550 nm (Schott 0G550) the flash produced no change in the composition of the 2BQ solution and no change in the agonist-induced current. This effect was due to the wavelength of the light and not to the increased intensity of the light as the wavelength of irradiation was increased: a neutral density filter placed in the light path reduced the amplitude of the total relaxation but did not change the relative amplitudes of the two components.

As the 2BQ solution bathing the electroplaque approached the photostationary state, a flash produced transient but no permanent conductance changes. Thus, at the CPSS the two components had equal but opposite amplitudes.

The relaxation rate constants for both components were measured. For a discussion of the rate constant of component 1_{l-f} and its properties see the previous section on visible-light flashes. The rate constant measured for component 2_{l-f} was a factor of 10-100 smaller than that measured for

Figure 12

The four traces represent light-flash relaxations with varied wavelengths of irradiation. Trace a had no flash-induced relaxation (λ>550 nm). Trace b had no measurable agonist-induced current increase after the flash (λ = 341 $\pm$ 10 nm). Trace c had a large agonist-induced current increase (λ = 400 $\pm$ 55 nm). Trace d had a very small conductance increase followed by the largest net agonist-induced current decrease (λ = 328 $\pm$ 47 nm). The amplitudes and relaxation rate constants are listed in Table 3. The measured current amplitude before the flash is shown between the left pair of cursors (just before the flash). The steady-state value is measured at the end of each trace between the right pair of cursors. Each trace was measured in the presence of 1 mM Carb and 2 μM of the *trans* photostationary state of 2BQ at 6°C. The voltage-jump relaxation was subtracted from each trace.

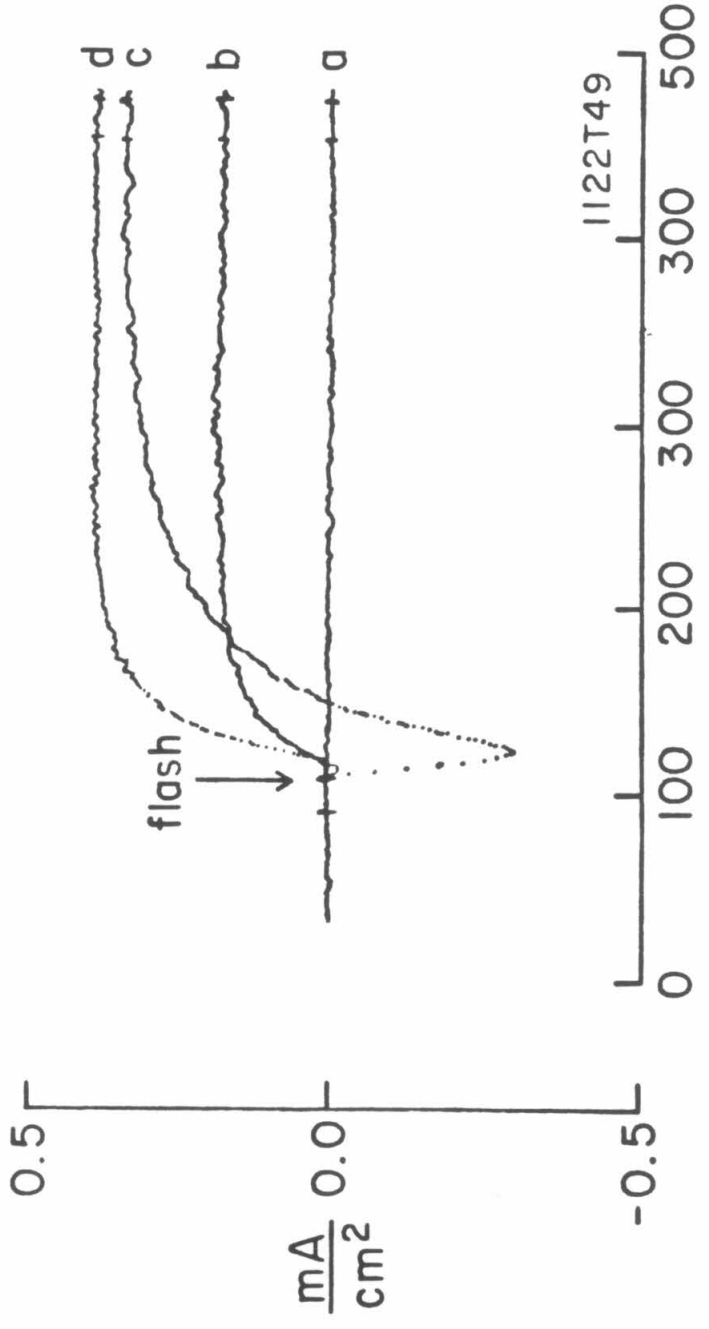
d
c
b
a
flash
0.5
0.0
-0.5
mA/cm²
0
100
200
300
300
500
msec
1122T49

Table 3

Light flashes of various wavelengths produced differing relaxations in cells exposed simultaneously to 1 mM Carb and to 2 μM of the *trans* photostationary state of 2BQ at -150 mV and 6°C (Fig. 12). The amplitude of the fast increase in agonist-induced current increased as the wavelength of irradiation increased toward 450 nm (relative maximum of *cis*-2BQ absorbance spectrum). The net decrease in agonist-induced current was dependent upon the wavelength and intensity of the irradiation. The rate constant of the decrease in agonist-induced current (component 2_{1-f}) depended upon the amplitude of the net current decrease and the wavelength of the irradiation.

Filter	Wavelength (±HWHM)	Relative Amplitude Component 1_{l-f}	Net Decrease in Agonist-Induced Current	Relaxation Rate Constant Component 2_{l-f}
341nm Interference	341 ± 10nm	< 10%	.19mA/cm^2 (Fig. 13b)	.018/ms
UG11 (UV)	328 ± 47nm	< 10%	.42mA/cm^2 (Fig. 13d)	.020/ms
UG1 (UV)	362 ± 33nm	20%	.64mA/cm^2	.021/ms
BG3 (Blue)	400 ± 55nm	45%	.36mA/cm^2 (Fig. 13c)	.010/ms
No Filter	300–800nm	100%	0 mA/cm^2 (Fig. 7)	.006/ms
OG550 (Orange)	>550nm	no relaxation	0 mA/cm^2 (Fig. 13a)	

component 1.

The relaxation rate constant was independent of voltage and the nature of the agonist. The relaxation rate constant of component 2_{1-f} was, however, dependent upon the concentration of *cis*-2BQ, agonist activity and temperature (Fig. 14). As the agonist concentration was increased at fixed 2BQ concentration, the rate constant measured for component 2_{1-f} decreased (Fig. 14). This was true for all three agonists tested. The change in the measured rate constant with agonist concentration decreased most rapidly at low-agonist concentrations and tended to saturate at high-agonist concentrations. Because the amplitude of component 2_{1-f} was quite small at both low- and high-agonist concentrations, the exact form of the decrease could not be determined. The data are consistent with a reduction in the rate constant equivalent to that produced by reducing the *cis*-2BQ concentration by a factor $(1 + [A]/K_a)$. Because the sequential binding model for agonist and antagonist receptor interaction assumes similar binding sites, agonist molecules can inhibit *cis*-2BQ binding in the same manner that 2BQ inhibits agonist binding. The models in the Appendix are consistent with the assumption that agonists reduce the antagonist activity by the factor$(1 + [A]/K_a)$.

The relaxation rate constant of component 2_{1-f} increased as the *cis*-2BQ concentration was increased. This increase in relaxation rate constant was seen in repetitive flashes in subsequent episodes (Fig. 13). The first flash produced the largest amplitude relaxation and the slowest rate of relaxation. The subsequent flashes produced smaller and smaller net decreases in agonist-induced current and larger and larger relaxation rate constants. After five flashes there was no further decrease in agonist-induced current (the 2BQ solution had reached the photostationary state). The amplitude of the decrease in current and the increase in relaxation rate constant are consistent with an exponential approach

Figure 13

Four sequential flash-induced relaxations on the same cell. The amplitude of the net decrease in agonist-induced current was reduced and the amplitude of component I_{I-f} (transient increase in agonist-induced current) was increased for the first (1) to the last (4) flash. The traces were taken in 500 μM Carb and 3 μM of the *trans* photostationary state of 2BQ at -150 mV and 20°C. Note the time scale change after 15 ms. The relaxation rate constants were 0.26/ms (1), 0.30/ms (2), 0.29/ms (3), and 0.33/ms (4). The standard errors were ± 10%. Each current trace is offset to superimpose the traces before the flash.

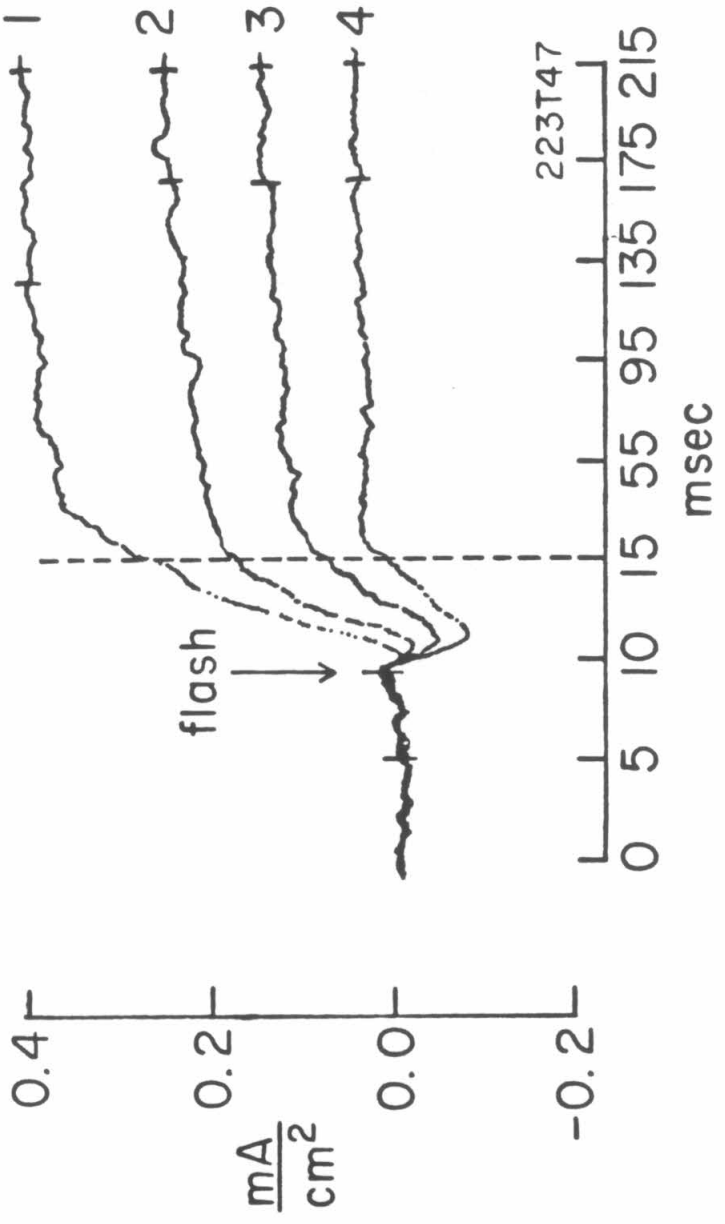
1
2
3
4
flash
223T47
0 5 10 15 55 95 135 175 215
msec
0.4
0.2
0.0
-0.2
mA/cm²

Figure 14

The relaxation rate constant of the slow decrease in agonist-induced current, after a UV-flash, was plotted versus the concentration of the *trans* photostationary state of 2BQ before the flash. The flash produced an increase in the mole-fraction of *cis*-2BQ from 0.20 to 0.49. The three lines are least-squares fit of data from 150 μM Carb (-150 mV) (●), 250 μM Carb (-90 mV) (■), and 400 μM Carb (-150 mV) (▲). All data were taken at 6°C. The zero concentration intercept of the three lines .011/ms (●), .0115/ms (■), and .0094/ms (▲), provide an estimate of the *cis*-2BQ dissociation rate constant. The relaxation rate constant increased with 2BQ concentration and decreased with agonist concentration.

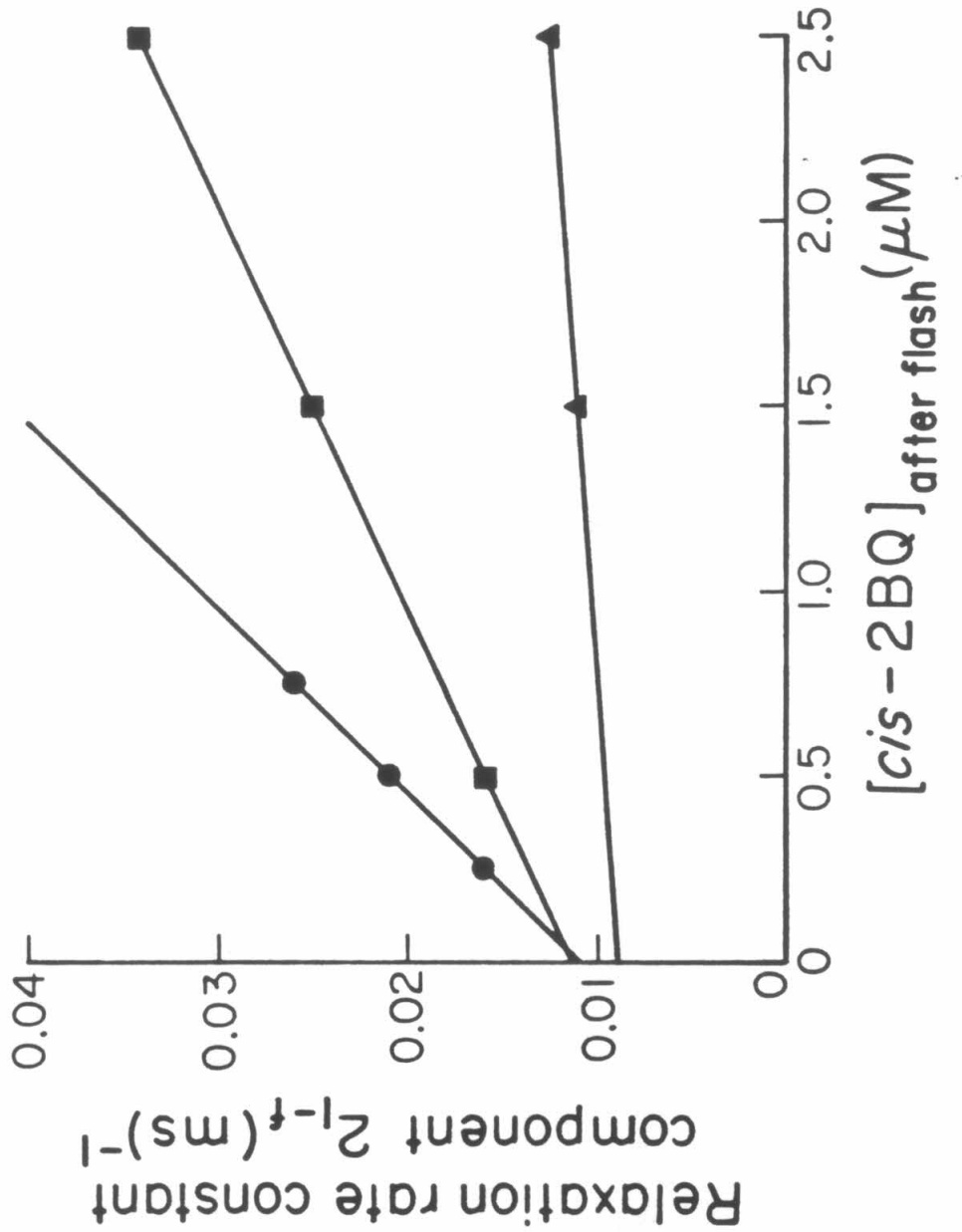
Relaxation rate constant
component $2l_{-f}(ms)^{-1}$
0.04
0.03
0.02
0.01
0
0
0.5
1.0
1.5
2.0
2.5
$[cis-2BQ]_{after\ flash}(\mu M)$

to the steady-state in parallel with the approach to the CPSS. (As mentioned earlier these consecutive flashes also caused an increase in the amplitude of component 1_{l-f} until component 1_{l-f} and component 2_{l-f} had the equal but opposite amplitudes.)

Because the flash intensity does not vary from trial to trial, the *cis*-2BQ concentration, after the light flash, can be changed by varying the concentration of TPSS-2BQ before the flash. The measured rate constant for component 2_{l-f} increased linearly with the TPSS-2BQ concentration (Fig. 14). A complete dose-rate plot was not possible because of the small amplitude of the light-flash relaxation at low and high 2BQ concentrations (Nargeot *et al.*, 1982). Therefore, the data points cluster about the 2BQ concentration which gave half maximal response with a fixed agonist concentration. (See Appendix for complete theoretical dose-rate plots.) From the abbreviated dose-rate plots an estimate of the dissociation rate constant for *cis*-2BQ was obtained. The line fit through the data points intercepts the y-axis at the dissociation rate constant (Lineweaver & Burke, 1934). The dissociation rate constant was found to be independent of the nature of the agonist and the voltage. This molecular rate constant had a Q_{10} of 3.4 between 6° and 20°C.

The slope of the dose-rate curves provided an estimate of the binding rate constant. However, the exact nature of the reduction in antagonist activity with agonist present was not known and was therefore fit to the data. The details involve two equations and two unknowns with one of the unknowns being the association rate constant. A second method was used which assumed that the equilibrium binding constant of *cis*-2BQ equals the dissociation rate constant divided by the binding rate constant. From the measured value of the dissociation rate constant (60.4/s at 20°C) and the equilibrium binding constant of *cis*-2BQ (0.33 μm), the association rate constant is 1.8×10^8/M/s (Table 4).

This agrees with a value of 1.6×10^{8}/M/s estimated from the slope of the dose-rate curves.

Table 4

The dissociation rate constant of *cis*-2BQ was obtained from the zero-concentration intercept of dose-rate plots like those of Fig. 14. The intercept was independent of voltage and agonist concentration. Values obtained in Sub and Carb at the same temperature were identical. The association rate constant was estimated by dividing the dissociation rate constant K_i estimated for the *cis* isomer.

Molecular Rate Constants of *cis*-2BQ

Agonist	Voltage	Concentration	Dissociation Rate Constant $k_-(s^{-1})$	Association Rate Constant $(M \cdot s)^{-1}$ $k_+ = 3 \times 10^6 \cdot k_-$
Carbachol (6°C)	-150 mV	150 μM	11.0 (1)	3.3×10^7
	- 90 mV	250 μM	11.4 ± 0.6 (2)	3.4×10^7
	-150 mV	400 μM	9.6 (1)	2.9×10^7
	-150 mV	1 mM	10.5 ± 0.7 (2)	3.2×10^7
Mean ± SD			10.7 ± 0.8 (6)	$3.2 \pm 0.2 \times 10^7$
Carbachol (20°C)	-150 mV	150 μM	71.2 ± 14.2 (4)	2.14×10^8
	-150 mV	300 μM	68.0 (1)	2.04×10^8
	-150 mV	400 μM	57.0 ± 13.7 (4)	1.71×10^8
Suberyldicholine (20°C)	-150 mV	10 μM	66.0 ± 4.5 (4)	2.00×10^8
	-150 mV	30 μM	44.8 ± 6.8 (4)	1.34×10^8
Mean ± SD			60.4 ± 13.9 (17)	$1.81 \pm 0.42 \times 10^8$

DISCUSSION

The data show that 2BQ inhibits nicotinic acetylcholine receptor activation in a manner consistent with competitive antagonist activity. The 2BQ molecule has the two important characteristics (a) that the *cis* and *trans* isomers differ in antagonist potency, and (b) that it can be photoisomerized between these two isomers. We have exploited these properties to study the kinetics of the interaction between *cis*-2BQ and the receptor; these kinetics have been interpreted in terms of the molecular rate constants for the association and dissociation events.

Both isomers display competitive antagonist activity and, therefore, a concentration jump from zero antagonist activity could not be produced. Such an experiment would measure the kinetic pathway from the open channel to the inhibited channel. Fortunately, other experiments probe the nature of the antagonist association reaction. Step increases in antagonist activity measured the rate-limiting step for channel closing and antagonist association. Step decreases in antagonist activity probed the dissociation of the competitive antagonist and the subsequent channel opening. The antagonist-receptor complex could be probed directly with a flash, revealing both the channel opening rate constant and the antagonist binding rate constant in a single relaxation.

2BQ as a competitive antagonist

The dose-response data, i.e., the parallel shift in the dose response curves and the equality of the maximum agonist-induced current in the presence and absence of 2BQ, are consistent with competitive antagonist activity at 2BQ concentration less than 3 μM and voltages less negative than -150 mV. It was not

possible, however, to exclude the possibility that 2BQ is only a noncompetitive antagonist and there was a large excess of "spare receptors" (receptors that activate at higher and higher agonist concentrations). Sheridan and Lester (1977) performed more complete studies on the agonist-receptor interaction under similar conditions and have shown that the approach to saturation displays no evidence of "spare-receptor" phenomena.

In addition, 2BQ does exhibit a form of noncompetitive antagonism, open channel blockade. However, this complication was not serious because the rate of blockade was slow at 2BQ concentrations less than 3 μM and at voltages less negative than -150 mV; and this effect could be subtracted from the measured agonist-induced current. If the local anesthetic effect were significant, light-flash relaxations would contain a step increase in current immediately following the flash because open, blocked channels should be unblocked when the molecule isomerizes. There is evidence for such step increases with EW-1 (Krouse, unpublished observations) and nifedipine (Gurney & Nerbonne, personal communication). Because the size of the step is proportional to the number of blocked, open channels and no step increase was seen in our experiments, we concluded that there was little open channel blockade during an episode.

Equilibrium binding constants

The equilibrium binding constant for the 2BQ-receptor interaction was calculated from dose-ratio studies. As mentioned in the Appendix, we assumed that there is the same number (2) of antagonist binding sites as agonist binding sites. This implies that there are three possible antagonist binding reactions which combine to form the measured equilibrium binding constant (K_i). If all three antagonist binding reactions had the same equilibrium binding constant (K_i), the dose-ratio plot would be linear with a slope equal to $1/K_i$. Theoretically, no other combination of dissociation constant would produce a

linear dose-ratio plot. However, the experimental results would be rather insensitive to departures from this situation. For instance, if the equilibrium binding constant of the singly to doubly bound antagonist-receptor interaction is varied, the dose-ratio plot remains nearly linear and the slope varies by less than 25% for a 10-fold change in the K_i. A second possibility is that the equilibrium affinity of both the antagonist binding to the single agonist-bound state and single antagonist-bound state are increased equally. In this case the slope of the dose-ratio plot roughly equals the new smaller equilibrium binding constant.

These possibilities can be summarized as follows. The K_i estimated from the slope of the dose-ratio plot is determined by the smaller of the two equilibrium binding constants for antagonist binding (a) to the unoccupied receptor or (b) to the single agonist-bound state. Experimentally, it was not possible to separate these two possibilities, because at very low or high agonist concentrations the response of the cell was less sensitive to variation in agonist concentration which introduces large errors into the dose-ratio plot.

(Component 1)

Immediately following a flash or voltage jump to more negative potentials, in the presence of 2BQ, a rapid ($\tau \sim 1$ ms) increase in conductance was observed and this increase (component 1) had all the properties of a voltage-jump relaxation in the absence of 2BQ. Because component 1 was not seen in the presence of photostable agonist alone, the most straightforward interpretation of this component is that the flash affects the bound as well as the free 2BQ molecules. The postulated mechanism accounting for components 1_{l-f} and 2_{l-f} is cartooned in Fig. 15. *cis*-2BQ molecules bound to the receptor isomerize upon absorbing of photons; the newly created *trans*-2BQ molecules dissociate, leaving receptors free to bind agonist; and channels open. Component 1_{l-f} should have the same properties as the voltage-jump relaxation, because both relaxations

Figure 15

A flash leads to photoisomerization of 2BQ molecules (b). Bound *cis*-2BQ molecules isomerize to *trans*-2BQ which leave the receptor (c), and agonist molecules in solution can then bind to the unoccupied receptor sites (c). Subsequent to the agonist binding, the channels open (d) producing the increase in voltage-clamp current associated with component 1.

After a normal opening channels close and agonist molecules unbind from the receptors (e). *cis*-2BQ molecules in solution are free to bind to the vacated sites (f) thus preventing agonist binding and reopening the channels. This return to the initial state (g) is termed component 2.

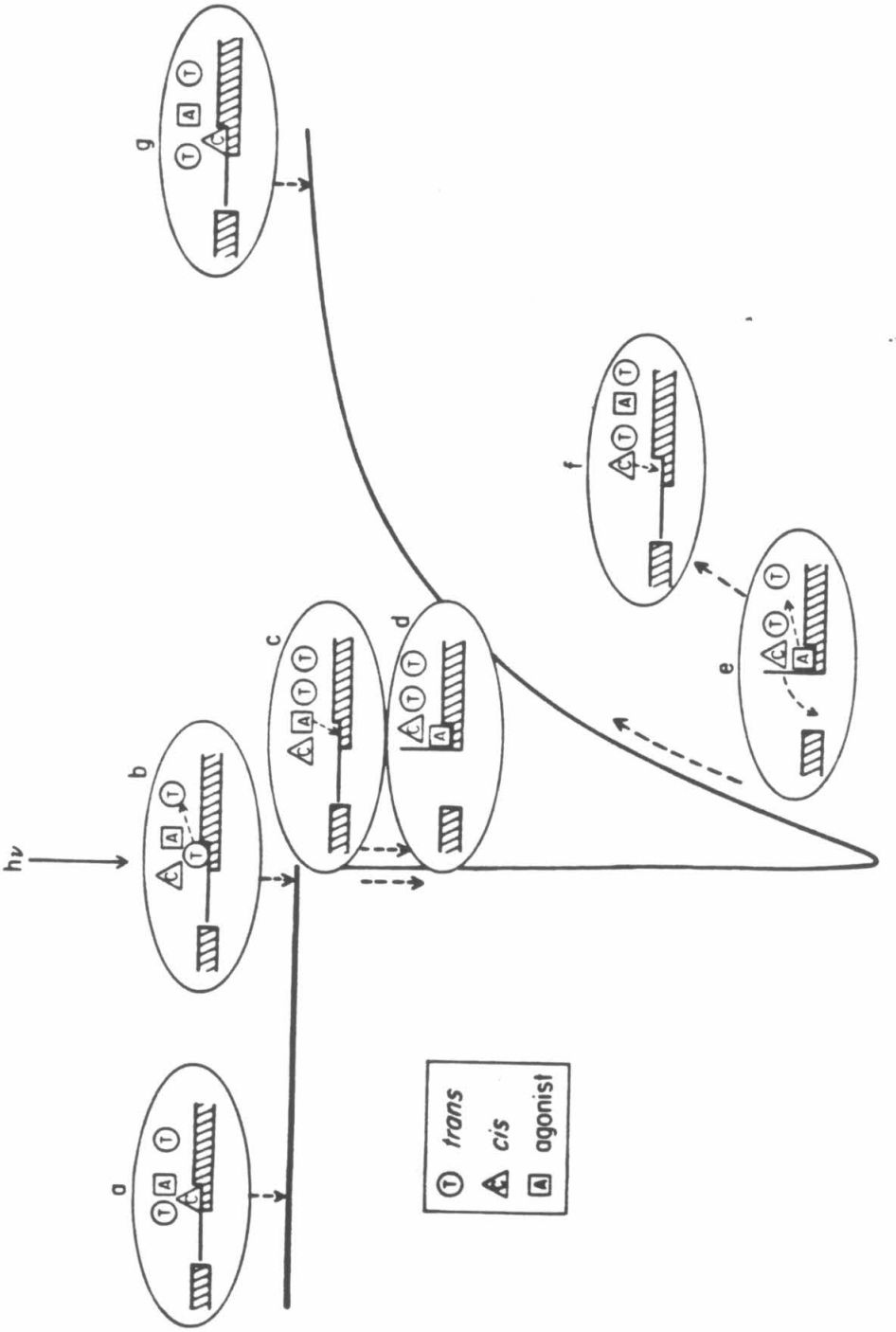
hν
a
b
c
d
e
f
g
T trans
C cis
A agonist

involve agonist binding to receptor molecules and subsequent channel opening, and the data bear this out.

Phenomena analogous to component 1_{l-f} have been previously reported for photoisomerizable agonists (Nass *et al.*, 1978; Lester *et al.*, 1980a). The interpretation in those experiments is that an agonist molecule immediately leaves the receptor upon absorption of a photon and the open channel closes. This is a molecular redistribution of the receptor molecules. Component 2_{l-f} was also seen in those experiments as the closed channels owing to component 1_{l-f} reopen with the time constant of the subsequent voltage-jump relaxation.

According to this view, the amplitude of component 1_{l-f} is determined by the number of 2BQ-receptor complexes that absorb a photon and isomerize. This conjecture is verified by experiments which revealed that the amplitude of component 1_{l-f} increased (a) as more receptors were inhibited, and (b) as the flash intensity was increased. The amplitude decreased as the agonist concentration increased or the cell was hyperpolarized, in agreement with the prediction that the amplitude of component 1_{l-f} is dependent on the number of inhibited channels.

(Component 2)

The slow relaxations attributed to 2BQ binding and unbinding, following flashes, permit the investigation of antagonist-receptor interactions. In the experiments described here, estimates of the dissociation rate constant were obtained. It was not possible to determine whether these rate constants pertain to (a) the receptor-antagonist ($I + R \rightleftharpoons IR$) interaction or (b) the single agonist-bound receptor-antagonist ($I + AR \rightleftharpoons AIR$) interaction or both. This ambiguity arises because both reactions led to inhibited receptors and their molecular rate constants equally determined the relaxation rate constant of phase 1 (Appendix, Fig. 22). The estimated dissociation rate constant for either reaction is an

underestimate of the true dissociation rate constant, because the dose-rate plots were fit with a line, and the predicted shape of the plot (Appendix, Fig. 17) has a sigmoid start. Therefore, the estimated dissociation rate constant may be too small by 10-20%.

The association rate constant was computed from the dissociation rate constant together with the equilibrium binding constant (K_i). If the dissociation rate constant is 10-20% too small, then the binding rate constant is also an underestimate of the true value. However, there is a further complication, because it was not possible to determine which antagonist binding reactions have the measured K_i and dissociation rate constant. If the results are from two different reactions, then the value of the binding rate constant has no meaning. Fortunately, the slope of the dose-rate plots confirm that the binding rate constant is roughly 1.6×10^8/M/s. This value agrees with the value of 1.8×10^8/M/s derived from the K_i measurements (Table 4).

Buffered diffusion

2BQ has a high affinity for the receptor and will be buffered as it diffuses in the synaptic cleft. This buffering will slow the diffusion rate of 2BQ by a factor $1 + (R/k_i)$ (Crank, 1956; Armstrong & Lester, 1979) where R is the concentration of receptor-binding sites in the cleft. Although the receptors are confined to the postsynaptic membrane, they effectively equilibrate rapidly with the 2BQ molecules in the cleft because the presynaptic membrane (~0.1 μ away) acts as a reflecting barrier. Thus, the diffusion of 2BQ should be slowed 1000-fold (1 + 330 μM/.33) by rebinding to its receptor. The Introduction discusses the use of the light-flash technique to minimize the effect of buffered diffusion. The Results support the hypothesis that buffered diffusion is not significant in light-flash experiments. The diffusion rate ($2 \times 10^5 \times K/\eta$) has a Q_{10} of 1.35 at room temperature, yet our measured dissociation rate constants have a Q_{10} of

3.3. Therefore, we can rule out a significant effect of diffusion on the measured rate constants.

Implications for curare

d-Tubocurarine is a classical competitive antagonist of the nicotinic acetylcholine receptor. The molecule is not photolabile and its interaction can be studied only with voltage jumps and iontophoretic pulses. Because the curare-receptor interaction is not voltage dependent, voltage-jump relaxations couple only weakly to the rate constants of interest. Iontophoretic pulses of d-tubocurarine reduce the amplitude of end-plate response, but within the synapse, the onset and recovery are slowed by buffered diffusion. Buffered diffusion has been reduced either with α-neurotoxins or by removing the presynaptic terminal; the results show an increased rate of action and recovery (Armstrong & Lester, 1979). Under the best conditions, experiments can measure only the rate constant for the receptor going from the open channel to the inhibited receptor or vice versa. In the case of d-tubocurarine the rate-limiting step for this pathway is channel opening and closing. Therefore, the rate constants of d-tubocurarine association and dissociation are not measurable in voltage-jump experiments. The effect of d-tubocurarine mimics that caused by a reduction in the concentration of agonist surrounding each receptor, thus reducing the amplitude and relaxation rate constant of a voltage-jump relaxation.

Voltage-jump relaxations have been stimulated (see Appendix for model and method of simulation, Fig. 19) for the simultaneous application of competitive antagonist and agonist. If the lifetime of the inhibited state is 30% or less of the open channel lifetime then the effect of the competitive antagonist is to reduce the amplitude and rate constant of the relaxation in a manner consistent with a reduction in agonist concentration. Conversely, if the

lifetime of the inhibited state is 10-fold larger than the open channel lifetime then the amplitude of the relaxation is reduced in a dose-dependent manner with no effect on the relaxation rate constant. These two simulations, with varied competitive antagonist molecular rate constants, reveal that curare must dissociate from the receptor 30 times faster than 2BQ. Therefore, the estimated association rate constant is roughly 4×10^9/M/s.

This estimated binding rate constant is very close to the encounter limited reaction rate constant of 6×10^9/M/s at room temperature. This would imply that each time a curare molecule encounters a receptor molecule, it binds to the receptor. Theoretically, it is possible that the forward binding rate constant need not be so large. The measured equilibrium binding constant may be for the antagonist-singly bound receptor state ($I + AR \rightleftharpoons AIR$) and the largest dissociation rate constant may be for the single antagonist bound state to the naked receptor. If, as suggested by other investigators (Neubig & Cohen, 1979; Sine & Taylor, 1981), curare has two different binding affinities, then the estimated rate constant would be too large by the ratio of the two binding affinities.

APPENDIX

Sequential Binding Model

1) $$IR \underset{k_{+4}}{\overset{k_{-4}}{\rightleftharpoons}} I + R + A \underset{k_{-1}}{\overset{k_{+1}}{\rightleftharpoons}} A\,R \underset{\alpha}{\overset{\beta}{\rightleftharpoons}} AR^*$$

Here IR represents the inhibited receptor

R represents the receptor molecule

AR represents the singly bound receptor

AR^* represents the open channel

let $K_1 = k_{-1}/k_{+1}$

$K_4 = k_{-4}/k_{+4}$

[A] = constant

$[R_t] = [IR] + [R] = [AR] + [AR^*]$

$[AR^*]/[R_t]$ = probability of being in the open state at equilibrium.

1a) $$= \beta[A]'/[(\alpha + \beta)[A]' + \alpha K_1]$$

Where $[A]' = [A]/(1 + [I]/K_4)$

2) $$2I + R + 2A \underset{k_{-1}}{\overset{k_{+1}}{\rightleftharpoons}} I + AR + A \underset{k_{-2}}{\overset{k_{+2}}{\rightleftharpoons}} A_2R \underset{\alpha}{\overset{\beta}{\rightleftharpoons}} A_2R^*$$

k_{+4} $\downarrow\uparrow$ k_{-4} $\qquad$ k_{+5} $\downarrow\uparrow$ k_{-5}

$$I + IR + A \underset{k_{-3}}{\overset{k_{+3}}{\rightleftharpoons}} AIR$$

k_{+6} $\downarrow\uparrow$ k_{-6}

I_2R

let $K_n = k_{-n}/k_{+n}$

$[R_t] = [I_2R] + [AIR] + [IR] + [R] + [AR] + [A_2R] + [A_2R^*]$

$$2a) \qquad [A_2R^*]/[R_t] = \frac{\beta[A]^2}{[(\alpha+\beta)[A]^2 + 2\alpha K_2\,[A](1+I_5)+\alpha K_1K_2\,(1+2I_4+I_4I_5)]}$$

where In = I/K_n

Equation 2a is plotted in Figure 17 as several log-dose response curves. In each panel the antagonist concentration was increased from 0 to 10 μM. Each panel was produced with K_1, K_2 and K_3 equal to 100 μM, K_4, K_5, K_6 equal to 1 μM and β/α equal to 10 except for the values printed in each panel. This figure mimics those found in figure 5.

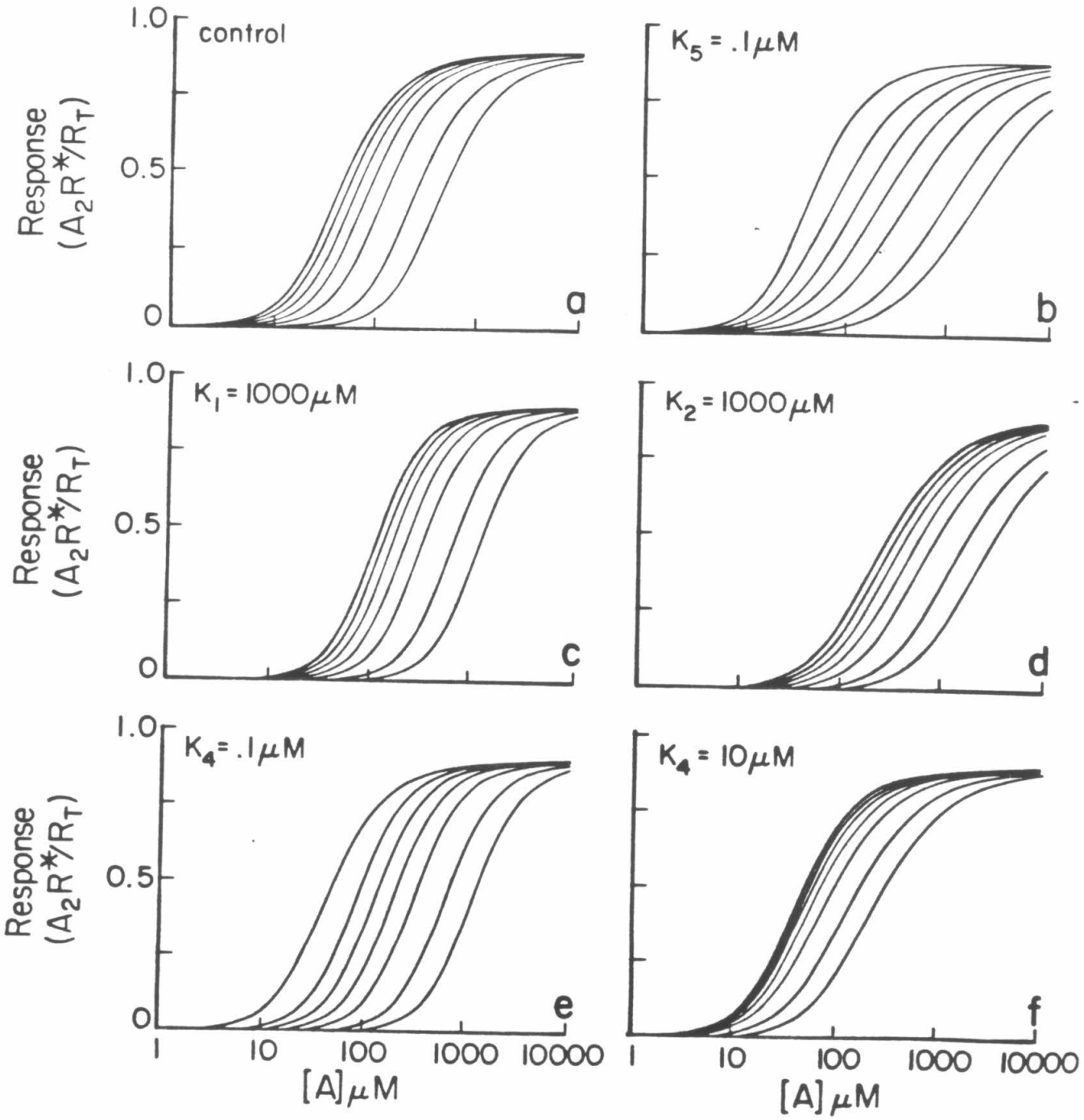
control
K_5 = .1μM
K_1 = 1000μM
K_2 = 1000μM
K_4 = .1μM
K_4 = 10μM
Response (A_2R^*/R_T)
1.0
0.5
0
a
b
c
d
e
f
1
10
100
1000
10000
[A]μM

Dose-Ratio Expression for Model 2

$$\frac{\beta[A]^2}{[(\alpha+\beta)\,[A]^{*2} + 2\alpha K_2\,[A] + \alpha K_1 K_2]} =$$

$$\frac{\beta[A]^{*2}}{[(\alpha+\beta)\,[A]^{*2} + 2\alpha K_2\,[A]^{*}\,(1+I_5) + \alpha K_1 K_2\,(1+2I_4 + I_4 I_5)]}$$

let $D = [A]^*/[A]$ = dose ratio

$A_1 = [A]/K_1$

3) $$D = \frac{2A_1\,(1+I_5) + \sqrt{4A_1^2\,(1+I_5)^2 + (8A_1+4)(1+2I_4+I_4I_5)}}{(4A_1+2)}$$

($D = 1 + [I]/K_4$ if $K_4 = K_5 = K_6$)

($D = 1 + [I]/K_4$ for Model 1)

Equation 3 has been plotted for several variations of the equilibrium constants for the antagonist binding in Figure 18. Trace 1 in each panel is the plot of D versus [I] when all these binding constants equal 1 μM. The other traces either increase (a) or decrease (b) the equilibrium binding constants by a factor of 10.

Trace	Change from trace 1	
2	a) K_4 = 10 μM	b) K_4 = 0.1 μM
3	a) K_6 = 10 μM	b) K_6 = 0.1 μM
4	a) $K_5 = K_6$ = 10 μM	b) $K_5 = K_6$ = 0.1 μM
5	a) K_5 = 10 μM	b) K_5 = 0.1 μM

A_1 was increased in parallel with I_4 in all traces.

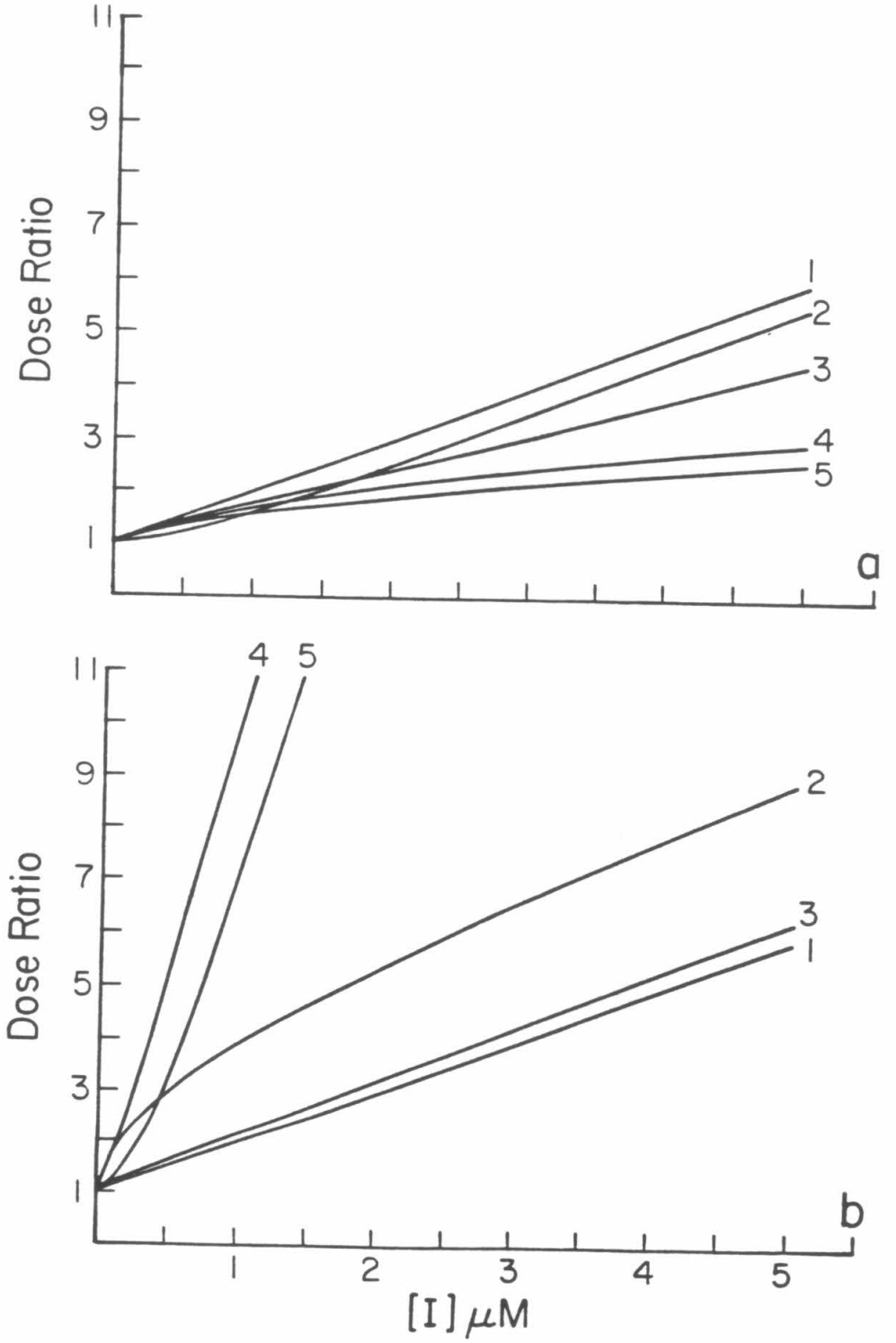
Dose Ratio
11
9
7
5
3
1
1
2
3
4
5
a
Dose Ratio
11
9
7
5
3
1
4
5
2
3
1
b
1
2
3
4
5
[I] μM

Maximum Flash Effect (Model 1)

$$x = \frac{\beta[A]}{[\alpha+\beta)\ [A] + K_1\alpha(1+I_4(1-\Delta))]} - \frac{\beta[A]}{[(\alpha+\beta)\ [A] + K_1\alpha\ (1+I_4)]}$$

$dx/d[A] = 0$

4) $A_1/(1+I_4) = \alpha/(\alpha+\beta)$ yields $[AR^*]/[R_t] = \beta/[2\cdot(\alpha+\beta)]$

Estimation of Light-Induced cis→trans Flux

Visible flash

$(k_{c\to t} + k_{t\to c}) = 3.0\ \text{flash}^{-1}$

$(k_{c\to t}/k_{c\to t} + k_{t\to c}) = 0.8\ \text{flash}^{-1}$

$k_{cis\to trans} = 2.4\ (91\%)$

$k_{trans\to cis} = .6\ (45\%)$

UV-only flash

$k_{cis\to trans} = .09\ (9\%)$

$k_{trans\to cis} = .51\ (40\%)$

Kinetic Simulations

Relaxations (light-flash and voltage-jump) were simulated from model 2 with a numerical simulation program for the IBM PC called TUTSIM (Applied i, Palo Alto, CA). The program numerically integrates simultaneous differential equations.

The simulations assume that the conformation change step ($A_2 \rightleftharpoons A_2R^*$) is the rate-limiting reaction for channel activation (α = 1/ms, β = 10/ms). Except where noted, the three antagonist equilibrium binding constants were equal and the antagonist rate constants were 10-fold smaller (0.1/ms) than the channel closing rate constant.

Figure 19 shows two simulated voltage-jump relaxations. At the 1 ms time point α is decreased from 1c/ms to 1/ms. In both trace a and b the number of open channels (A_2R^*) increased. Trace a shows two components. The faster increase represents agonist binding to unoccupied receptors and the slower increase results from inhibited channels becoming unoccupied, binding agonist, and finally opening. Trace b includes both of these processes plus a very slow (.01/ms) local anesthetic effect of the inhibitor. This trace mimics many of the voltage-jump experiments and details the method by which the amplitude of the voltage-jump relaxation was estimated. The actual and estimated amplitudes differ by less than 10% and the voltage-jump relaxation nearly superimpose for the initial 70% of the relaxation.

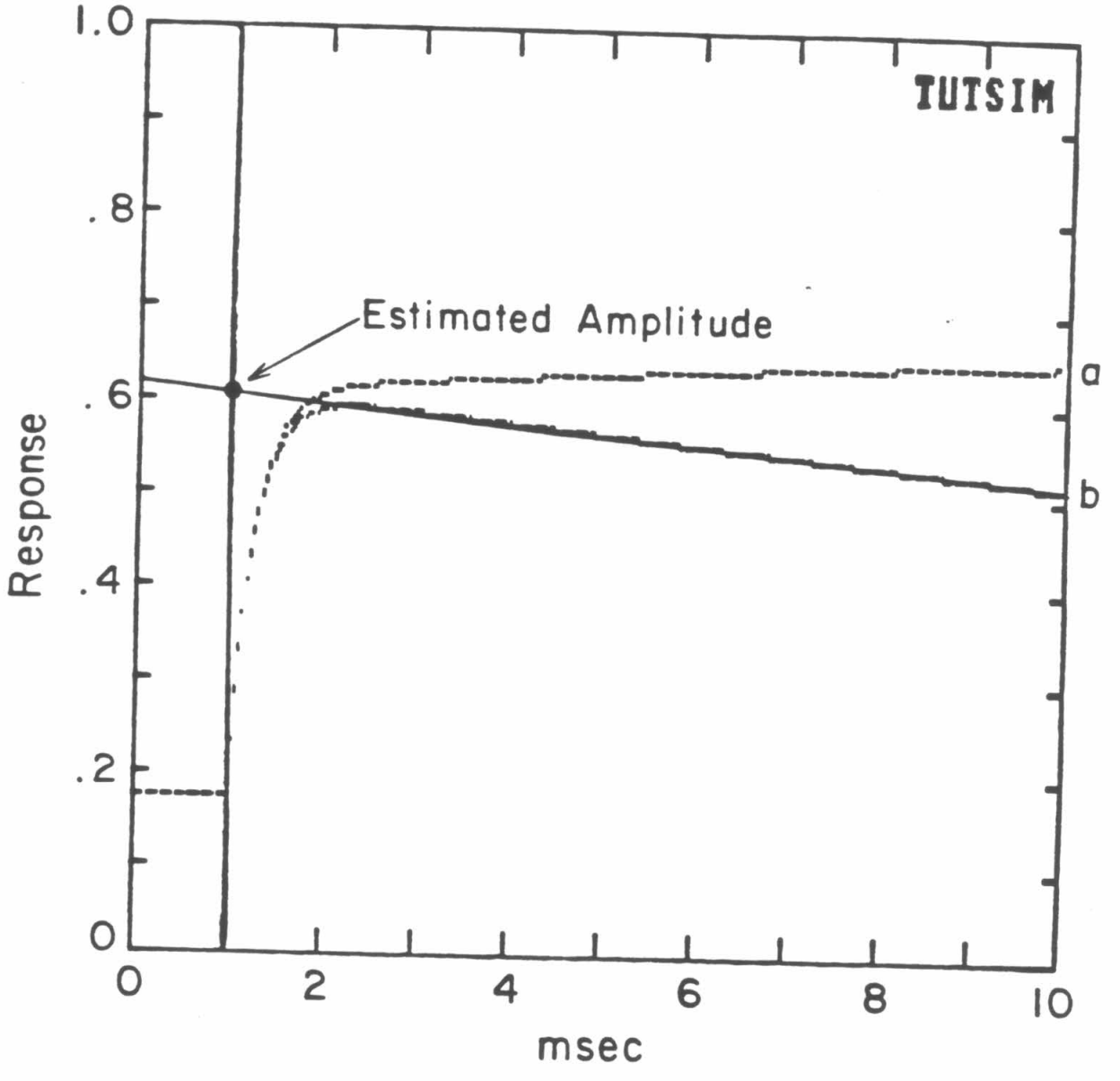
TUTSIM
Estimated Amplitude
a
b
Response
1.0
.8
.6
.4
.2
0
0
2
4
6
8
10
msec

Figure 20 simulates the effect of varying the antagonist rate constants on the voltage-jump relaxations. All three panels contain two voltage-jump relaxations, (i) in the presence of agonist alone and (ii) in the simultaneous presence of antagonist and an increased agonist concentration ($A' = A \cdot (1 + [I]/K_i)$). Figure 20a shows two relaxations if the inhibitor unbinding rate constant is 3-fold larger than α. Figure 20b assumes that the antagonist unbinding rate constant equals the channel closing rate constant. Figure 20c assumes that the antagonist unbinding rate constant is 1/3 of α. Figure 20c has two components, the faster of which is similar to a voltage jump in the increased agonist concentration only.

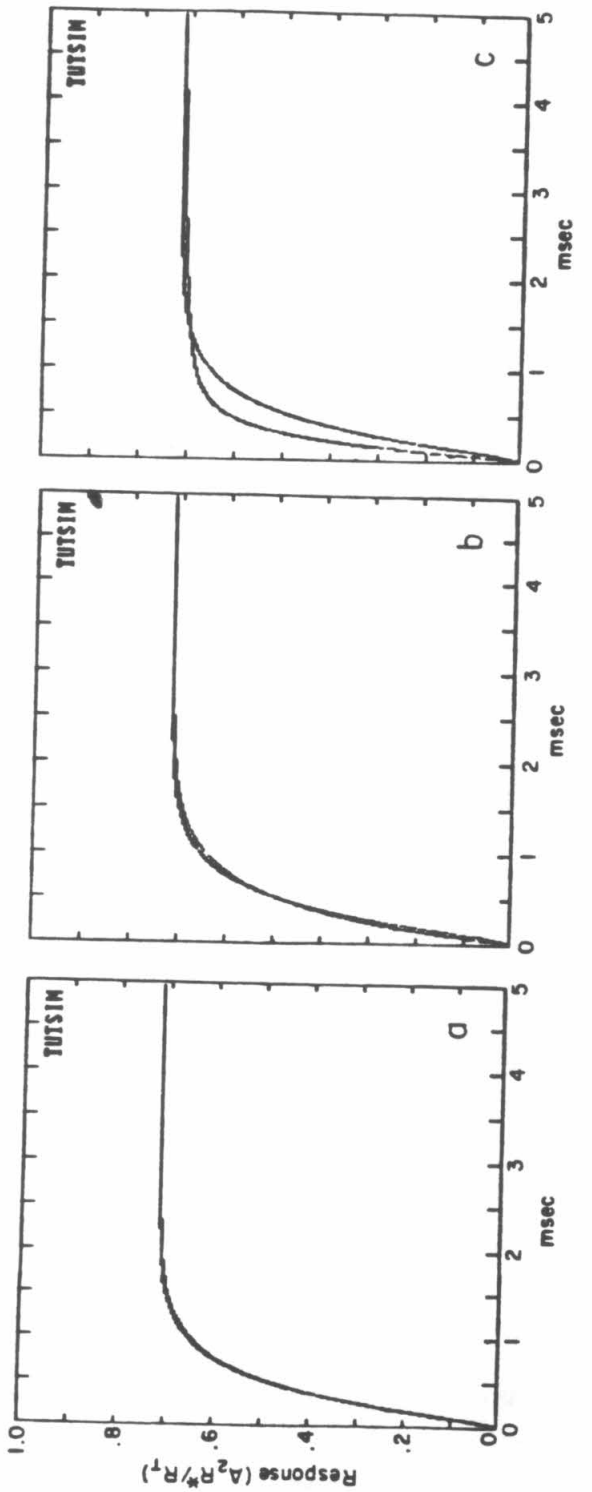
TUTSIM
a
b
c
msec
Response (A_2R^*/R_T)
0
.2
.4
.6
.8
1.0
1
2
3
4
5

Figure 21 simulates a flash which produces no net change in the 2BQ composition. Component 1_{1-f} and 2_{1-f} have equal but opposite amplitudes and the relaxation rate constants differ by a factor of roughly 20. This simulation attempt to mimic the results shown in Fig. 10.

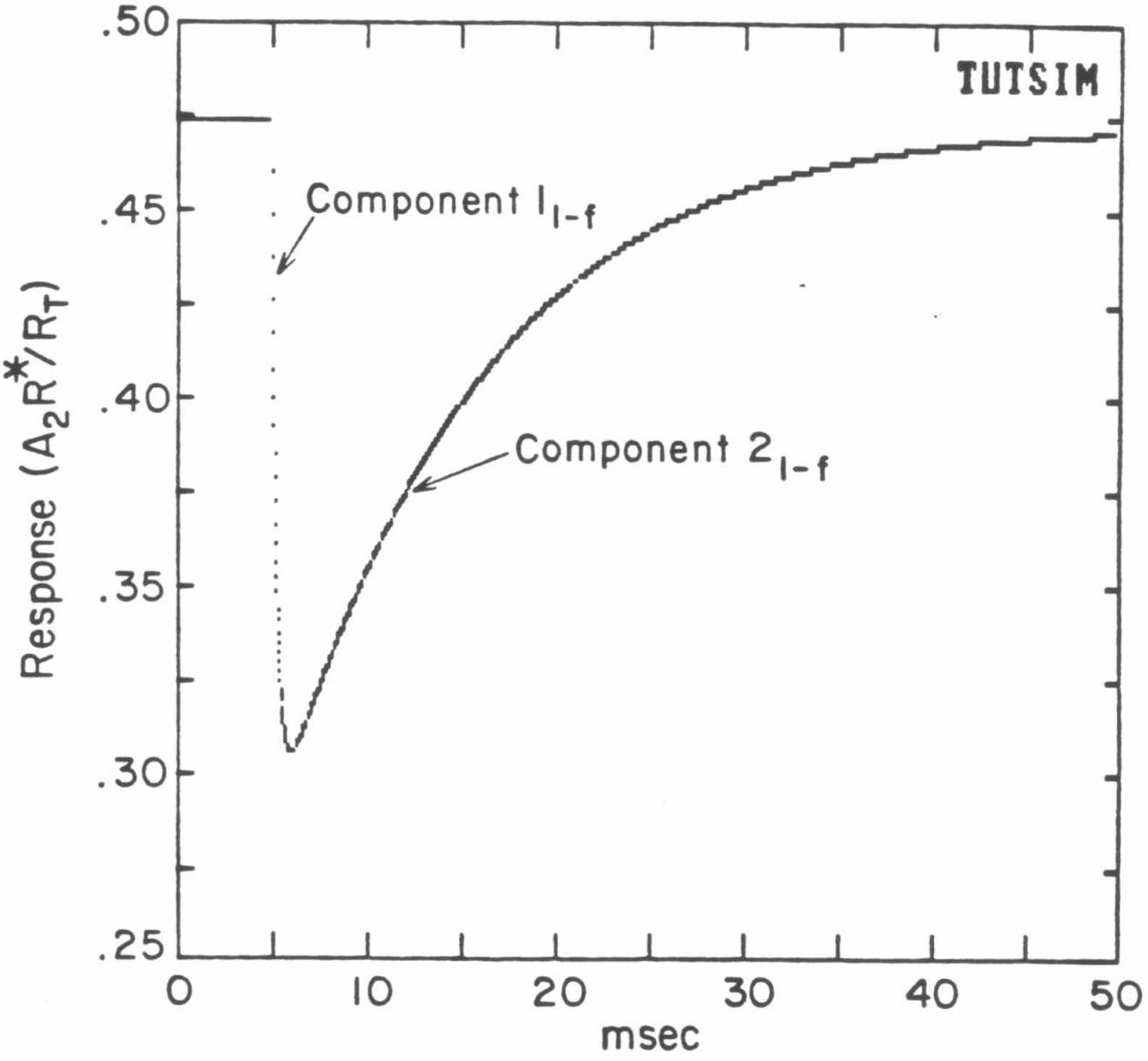
.50
.45
.40
.35
.30
.25
0
10
20
30
40
50
msec
Response (A_2R^*/R_T)
TUTSIM
Component 1_{1-f}
Component 2_{1-f}

Figure 22 simulates the effect of varying the wavelength of irradiation on the flash relaxation. The four traces vary in their effect on the bound 2BQ molecules. Trace c assumes that half of the 2BQ-receptors are affected, while trace d assumes that only 10% of the 2BQ-receptor complexes are disturbed. This simulation mimics the results shown in Fig. 12. Notice that in this simulation the relaxation rate is not strongly dependent upon the 'wavelength' of irradiation. This discrepancy may be simulated if two distinct competitive antagonists exist for the receptor (cis and trans) and one antagonist has slower kinetics than the other.

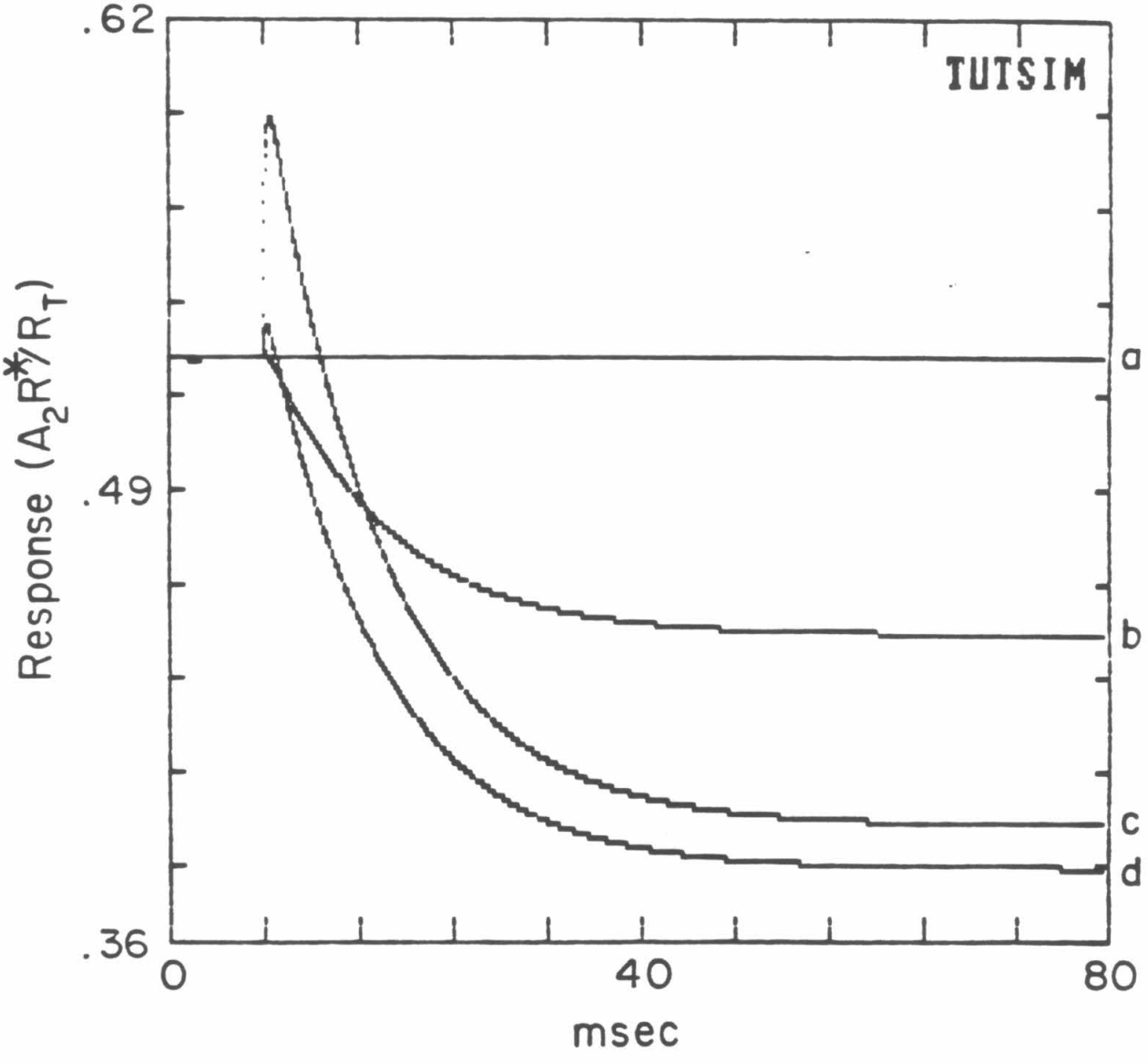
TUTSIM
.62
.49
.36
Response (A_2R^*/R_T)
0
40
80
msec
a
b
c
d

Simulating the hypothetical experiment of a concentration jump of the antagonist from zero concentration revealed a sigmoid start to the flash-induced relaxations. The 'delay' after the jump was dependent upon the final antagonist concentration (Fig. 23). The agonist concentration was equal to $k_d/2$ (50 μM). This experiment was not possible on the electroplaque because of the presence of component 1_{1-f} in all light-flash relaxations. This simulated 'delay' is also caused by component 1_{1-f} but the amplitude is such that the amplitude of component 1_{1-f} + component 2_{1-f} equals zero following the flash.

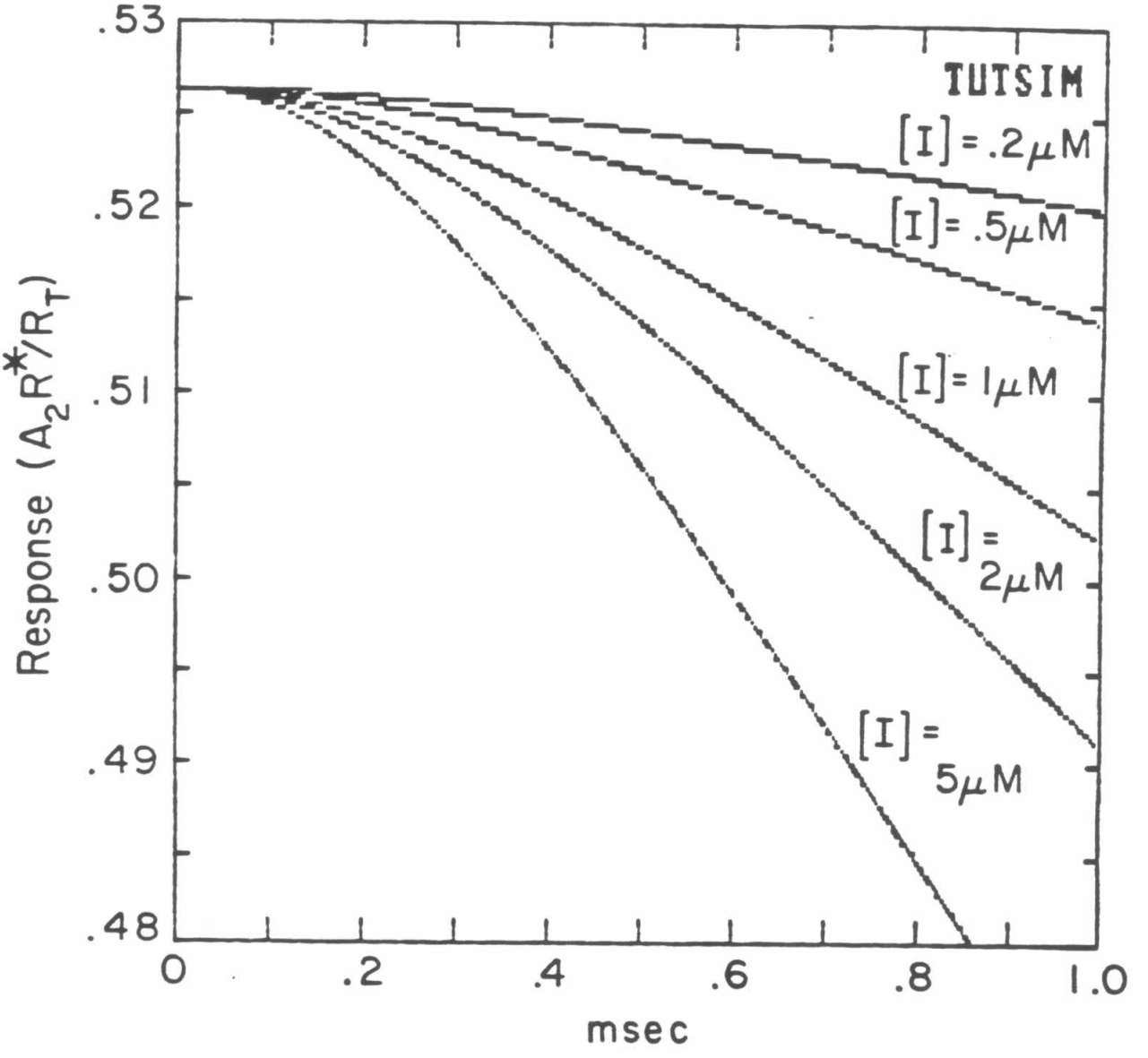
TUTSIM
[I] = .2μM
[I] = .5μM
[I] = 1μM
[I] = 2μM
[I] = 5μM
Response (A_2R^*/R_T)
.53
.52
.51
.50
.49
.48
0
.2
.4
.6
.8
1.0
msec

Flash-relaxations, which resulted from an increase of antagonist concentration, were also simulated. These relaxations start from zero antagonist concentration. Figure 24 shows three flash-induced conductance decreases. The agonist concentration for these three simulations was 100 μM. The three traces differ in the rate constants of the antagonist-receptor interaction. If the rate constants are equal ($k_{-4} = k_{-5}$, $k_{+4} = k_{+5}$) then curve b results. If either of the two reactions ($I + R \rightleftharpoons IR$, $AR + I \rightleftharpoons AIR$) is slowed by a factor of 3 (curve a) the relaxation rate constant is reduced by less than 5%. However, if either of the reactions is increased by a factor of 3 the relaxation rate increases dramatically. Therefore, the measured relaxation rate constant reflects the antagonist-receptor interaction that has the largest rate constants.

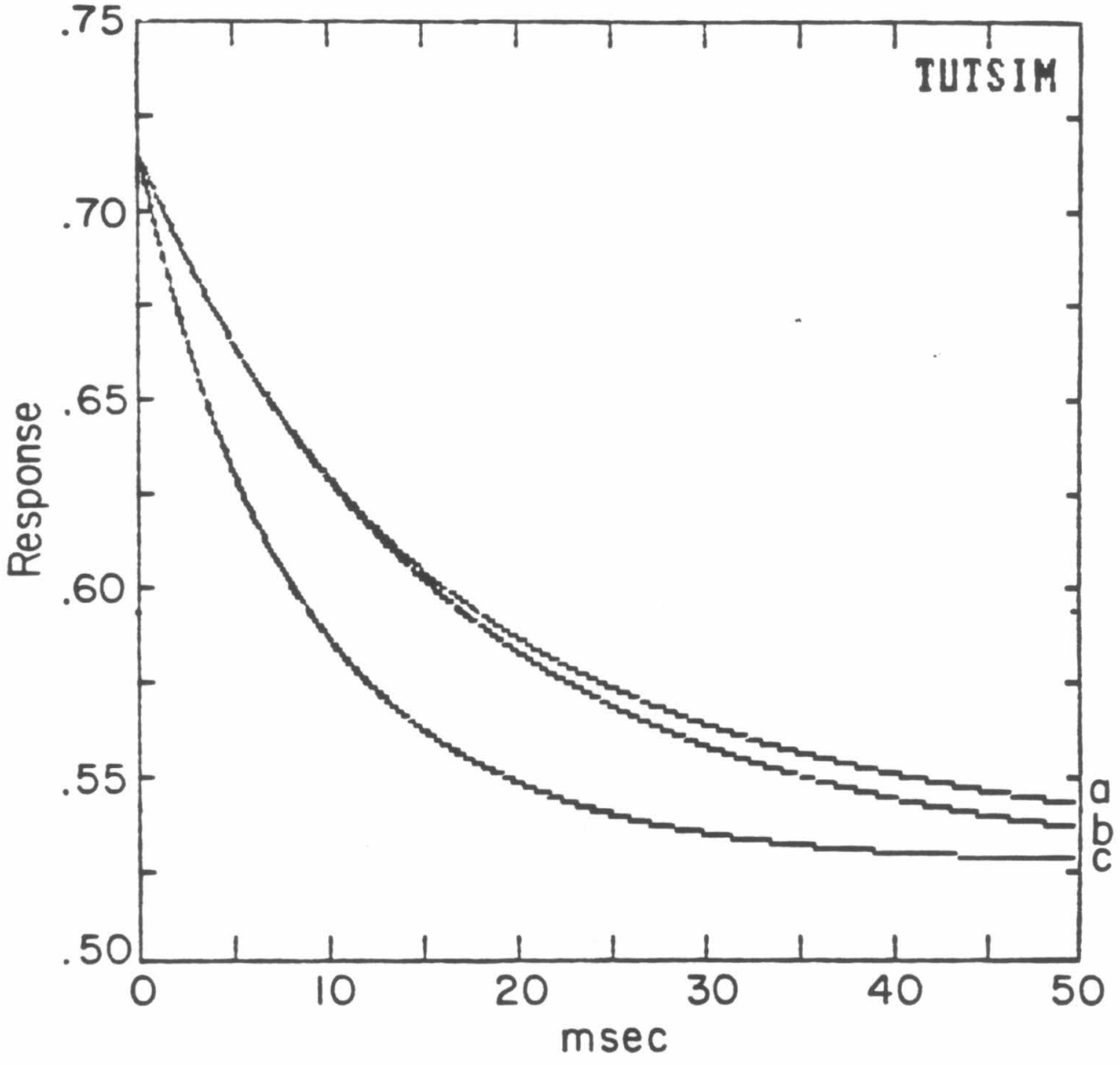
TUTSIM
.75
.70
.65
.60
.55
.50
Response
0
10
20
30
40
50
msec
a
b
c

Many UV-flash relaxations have been simulated and their relaxation rate constants measured. The data have been plotted as a dose-rate plot for varying agonist concentrations (Fig. 25). We assumed that the three antagonist binding reactions have equal rate constants. The dose-rate curves intersect the y axis at .05/ms. This was the antagonist dissociation rate constant. The slope at zero agonist concentration (curve derived theoretically) equaled twice the forward rate constant. This was expected because there are two binding sites. As the agonist concentration increases, the slope of the plots decreases and the nonlinear start becomes more pronounced at low-antagonist concentrations. This decrease in the slope of the linear part of the dose-rate plot is consistent with a reduction in antagonist concentration caused by the presence of the agonist ($[I]' = [I]/(1 + [A]/K_a)$). This figure confirms that the zero concentration intercept is the dissociation rate of the antagonist receptor complex. This simulation should be compared with the actual data in Fig. 14.

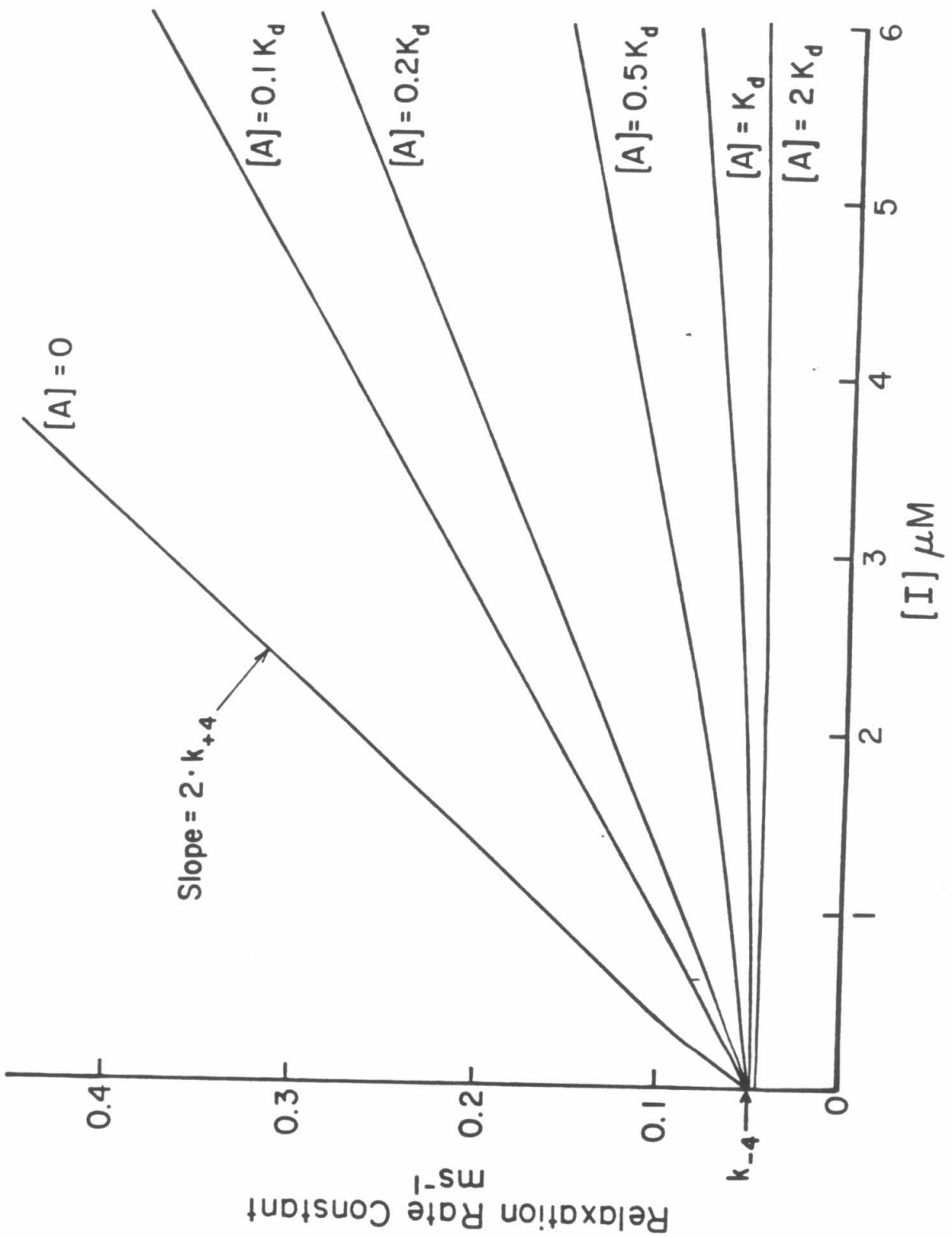
[A] = 0
[A] = 0.1 K_d
[A] = 0.2K_d
[A] = 0.5K_d
[A] = K_d
[A] = 2 K_d
Slope = 2 · k_+4
k_-4
0.4
0.3
0.2
0.1
0
1
2
3
4
5
6
[I] μM
Relaxation Rate Constant
ms^-1

Figure 26 simulates voltage jumps and light flashes for a competitive antagonist such as 2BQ (dissociation rate constant is small) and a competitive antagonist like curare (dissociation rate constant is large). In both cases the largest binding rate constant is 2×10^8/M/s. This simulation provides evidence for the hypothesis that curare need not bind and unbind rapidly in order that its kinetics not be measurable in relaxation experiments. The K_i for each simulation is roughly the same from dose-ratio analysis. In the simulation the two differences between the two curves are: the dissociation rate constant for the singly bound antagonist state (IR→I+R) and; the affinity of the antagonist for the unoccupied receptor (a factor of 10 less in the case of curare).

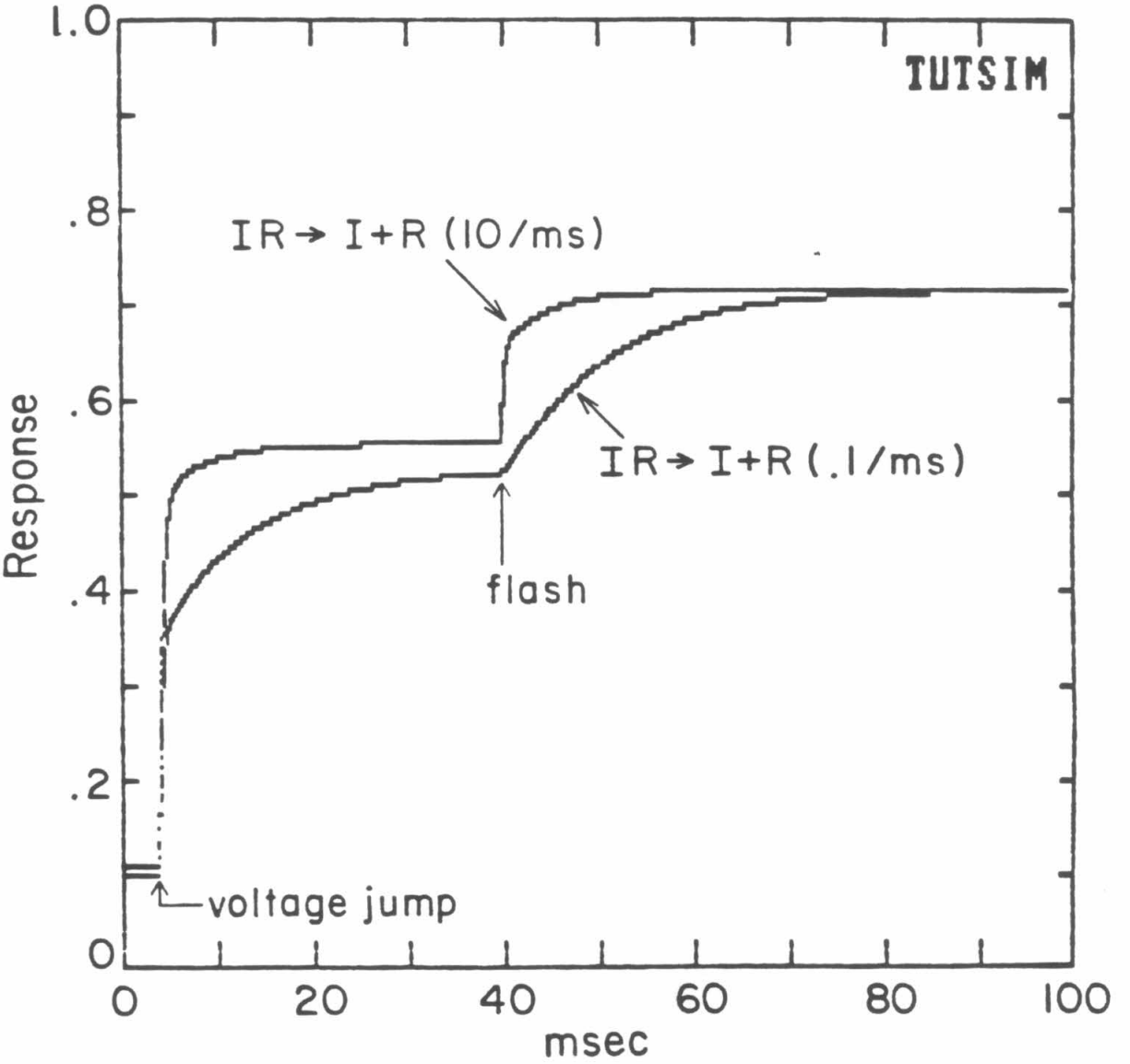
TUTSIM
IR → I+R (10/ms)
IR → I+R (.1/ms)
flash
voltage jump
Response
msec
1.0
.8
.6
.4
.2
0
0
20
40
60
80
100

References

Adams, P. R. 1975. Kinetics of agonist conductance changes during hyperpolarization at frog endplates. *Br. J. Pharmacol.* **53**:308-310.

Anderson, C. R. and C. F. Stevens. 1973. Voltage clamp analysis of acetylcholine induced end-plate current fluctuations at frog neuromuscular junction. *J. Physiol. (Lond.).* **235**:655-691.

Armstrong, D. L. and H. A. Lester. 1979. The kinetics of tubocararine action and restricted diffusion within the synaptic cleft. *J. Physiol. (Lond.).* **294**:365-386.

Bartels, E., N. H. Wassermann, and B. F. Erlanger. 1971. Photochromic activators of the acetylcholine receptor. *Proc. Natl. Acad. Sci. USA* **68**:1820-1823.

Colquhoun, D., F. Dreyer, and R. E. Sheridan. 1979. The actions of tubocurarine at frog neuromuscular junction. *J. Physiol. (Lond.).* **293**:247-284.

Crank, J. 1956. *Mathematics of Diffusion.* Oxford: The Clarendon Press.

Del Castillo, J. and B. Katz. 1957. A study of curare action with an electrical micro-method. *Proc. R. Soc. Lond. Ser. B. Biol. Sci.* **146**:339-356.

Gaddum, J. H. 1937. The quantitative effects of antagonist drugs. *J. Physiol. (Lond.).* **89**:7-9P.

Heidmann, T. and J-P. Changeux. 1978. Structural and functional properties of the acetylcholine receptor protein in its purified and membrane-bound states. *Ann. Rev. Biochem.* **47**:317-357.

Jenkinson, D. H. 1960. The antagonism between d-tubocurarine and substances which depolarize end-plates. *J. Physiol. (Lond.).* **152**:309-324.

Katz, B. and R. Miledi. 1972. The statistical nature of the acetylcholine potential and its molecular components. *J. Physiol. (Lond.).* **224**:665-699.

Katz, B. and R. Miledi. 1978. A re-examination of curare action at the motor endplate. *Proc. R. Soc. Lond. Ser. B* **203**:119-133.

Krouse, M. E., H. A. Lester, B. F. Erlanger, and N. H. Wassermann. 1982. A study of the nicotinic acetylcholine receptor using a photoisomerizable competitive antagonist. *Soc. Neurosci. Abstr.* **8**:498.

Langley, J. N. 1905. On the reaction of cells and of nerve endings to certain poisons, chiefly as regards the reaction of striated muscle to nicotine and to curare. *J. Physiol. (Lond.)* **33**:374-413.

Lester, H. A. and H. W. Chang. 1977. Response to acetylcholine receptors to rapid, photochemically produced increases in agonist concentration. *Nature (Lond.)* **266**:373-374.

Lester, H. A., M. E. Krouse, M. M. Nass, N. H. Wassermann, and B. F. Erlanger. 1980a. A covalently bound photoisomerizable agonist: comparison with reversibly bound agonists at *Electrophorus* electroplaques. *J. Gen. Physiol.* **75**:207-232.

Lester, H. A., M. M. Nass, M. E. Krouse, J. M. Nerbonne, N. H. Wassermann, and B. F. Erlanger. 1980b. Electrophysiological experiments with photoisomerizable cholinergic compounds. Review and progress report. *Ann. N.Y. Acad. Sci.* **346**:475-490.

Lineweaver, H. and D. Burk. 1934. The determination of enzyme dissociation constants. *J. Amer. Chem. Soc.* **56**:658-666.

Magleby, K. L. and C. F. Stevens. 1972a. The effect of voltage on the time course of end-plate currents. *J. Physiol. (Lond.)* **223**:151-171.

Magleby, K. L. and C. F. Stevens. 1972b. A quantitative description of end-plate currents. *J. Physiol. (Lond.).* **223**:173-197.

Manalis, R. S. 1977. Voltage-dependent effect of curare at frog neuromuscular junction. *Nature (Lond.).* **267**:366-368.

Morris, C. E., M. B. Jackson, H. Lecar, and B. S. Wong. 1982. Activation of individual acetylcholine channels by curare in embryonic rat muscle. *Biophys. J.* **37**:19a.

Morris, C. E., B. S. Wong, M. B. Jackson, and H. Lecar. 1983. Single-channel currents activated by curare in cultured embryonic rat muscle. *J. Neurosci.* **3**:2525-2531.

Nargeot, J., H. A. Lester, N. J. M. Birdsall, J. Stockton, N. H. Wassermann, and B. F. Erlanger. 1982. A photo-isomerizable muscarinic antagonist. Studies of binding and of conductance relaxations in frog heart. *J. Gen. Physiol.* **79**:657-678.

Nargeot, J., J. M. Nerbonne, J. Engels and H. A. Lester. 1983. Time course of the increase in the myocardial slow inward current after a photochemically generated concentration jump of intracellular cAMP. *Proc. Natl. Acad. Sci. USA* **80**:2395-2399.

Nass, M. M., H. A. Lester, and M. E. Krouse. 1978. Response of acetylcholine receptors to photoisomerization of bound agonist molecules. *Biophys. J.* **24**:135-160.

Neher, E. and B. Sakmann. 1976. Single-channel currents recorded from the membrane of denervated frog muscle fibres. *Nature (Lond.).* **260**:799-802.

Nerbonne, J. M., R. E. Sheridan, L. D. Chabala, and H. A. Lester. 1983. cis-3,3'-bis-[a-(trimethylammonium)/methyl]azobenzene (cis-Bis-Q) Purification and properties at acetylcholine receptors of *Electrophorus* electroplaques. *Mol. Pharmacol.* **23**:344-349.

Neubig, R. R. and J. B. Cohen. 1979. Equilibrium binding of [^{3}H]tubocurarine and [^{3}H]acetylcholine by *Torpedo* postsynaptic membranes: stoichiometry and ligand interactions. *Biochemistry* **18**:5464-5475.

Noda, M., Y. Furutani, H. Takahashi, M. Toyosato, T. Tanabe, S. Shimizu, S. Kikyotani, T. Kayano, T. Hirose, S. Inayama, and S. Numa. 1983. Cloning and sequence analysis of calf cDNA and human genomic DNA encoding α-subunit precursor of muscle acetylcholine receptor. *Nature (Lond.)* **305**:818-823.

Raftery, M. A. 1973. Isolation of acetylcholine receptor-α-bungarotoxin complexes from *Torpedo californica* electroplax. *Archs. Biochem. Biophys.* **154**:270-276.

Raftery, M. A., M. W. Hunkapiller, C. D. Strader, and L. E. Hood. 1980. Acetylcholine receptor: complex of homologous subunits. *Science* **208**:1454-1456.

Rang, H. P. 1971. Drug receptors and their function. *Nature (Lond.).* **231**:91-96.

Sheridan, R. E. and H. A. Lester. 1977. Rates and equilibria at the acetylcholine receptor of *Electrophorus* electroplaques: a study of neurally evoked post-synaptic currents and of voltage-jump relaxations. *J. Gen. Physiol.* **70**:187-219.

Sheridan, R. E. and H. A. Lester. 1982. Functional stoichiometry of the nicotinic receptor. The photon cross-section for phase 1 corresponds to two Bis-Q molecules per channel. *J. Gen. Physiol.* **80**:499-515.

Sigworth, F. J. 1980. The conductance of sodium channels under conditions of reduced current at the node of ranvier. *J. Physiol. (Lond.).* **307**:131-142.

Sine, S. M. and P. Taylor. 1981. Relationship between antagonist occupancy and the functional capacity of the acetylcholine receptor. *J. Biol. Chem.* **256**: 6692-6699.

Takeuchi, A. and N. Takeuchi. 1960. On the permeability of the end-plate membrane during the action of transmitter. *J. Physiol. (Lond.)* **154**:52-67.

Tan, Y. and F. J. Barrantes. 1980. Fast kinetics of antagonist-acetylcholine receptor interactions: a temperature-jump relaxation study. *Biochem. Biophys. Res. Commun.* **92**:766-774.

Trautmann, A. 1982. Curare can open and block ionic channels associated with cholinergic receptor. *Nature (Lond.)* **298**:272-275.